Color superfluidity of neutral ultracold fermions in the presence of color-flip and color-orbit fields

Doga Murat Kurkcuoglu[1,2] and C. A. R. Sá de Melo[2]
[1]*Department of Physics, Georgia Southern University, Statesboro, Georgia 30460, USA*
[2]*School of Physics, Georgia Institute of Technology, Atlanta, Georgia 30332, USA*

(Received 1 August 2017; revised manuscript received 30 December 2017; published 22 February 2018)

We describe how color superfluidity is modified in the presence of color-flip and color-orbit fields in the context of ultracold atoms and discuss connections between this problem and that of color superconductivity in quantum chromodynamics. We study the case of s-wave contact interactions between different colors and we identify several superfluid phases, with five being nodal and one being fully gapped. When our system is described in a mixed-color basis, the superfluid order parameter tensor is characterized by six independent components with explicit momentum dependence induced by color-orbit coupling. The nodal superfluid phases are topological in nature and the low-temperature phase diagram of the color-flip field versus the interaction parameter exhibits a pentacritical point, where all five nodal color superfluid phases converge. These results are in sharp contrast to the case of zero color-flip and color-orbit fields, where the system has perfect U(3) symmetry and possesses a superfluid phase that is characterized by fully gapped quasiparticle excitations with a single complex order parameter with no momentum dependence and by inert unpaired fermions representing a nonsuperfluid component. In the latter case, just a crossover between a Bardeen-Cooper-Schrieffer and a Bose-Einstein-condensation superfluid occurs. Furthermore, we analyze the order parameter tensor in a total pseudospin basis, investigate its momentum dependence in the singlet, triplet, and quintet sectors, and compare the results with the simpler case of spin-1/2 fermions in the presence of spin-flip and spin-orbit fields, where only singlet and triplet channels arise. Finally, we analyze in detail spectroscopic properties of color superfluids in the presence of color-flip and color-orbit fields, such as the quasiparticle excitation spectrum, momentum distribution, and density of states to help characterize all the encountered topological quantum phases, which can be realized in fermionic isotopes of lithium, potassium, and ytterbium atoms with three internal states trapped.

DOI: 10.1103/PhysRevA.97.023632

I. INTRODUCTION

Ultracold atoms have become preferred systems to study experimentally, because they can be used as quantum simulators of various phenomena across different areas of physics. Today it is possible to engineer Hamiltonians in the laboratory that describe models that have been investigated in the context of condensed-matter physics. For instance, two very successful examples of these experimental quantum simulations are studies of the superfluid-insulator transition [1] and the evolution from Bardeen-Cooper-Schrieffer (BCS) to Bose-Einstein condensation (BEC) superfluidity [2–8], which were performed in recent years.

The success of cold atoms as quantum simulators is largely due to the flexibility that these systems have. It is now routinely possible to change atomic species, dimensionality, density, and interactions in clouds of ultracold atoms, while in the case of optical lattices, it is possible, in addition, to change the lattice structure. For instance, recent experimental advances lead to the trapping of three hyperfine states in Fermi gases, such as ^{6}Li, which have tunable interactions via an external magnetic field, which become SU(3) symmetric in the limit of high magnetic fields [9,10]. Even larger component systems have now been produced in the laboratory, such as in the case of the fermion isotope of ytterbium, ^{173}Yb, where six internal states exist with essentially SU(6) symmetry, which can be reduced to SU(3) by selectively trapping only three internal states [11]. Current temperatures that can be achieved in these systems are approximately $T = 0.3T_F$, where T_F is the Fermi temperature set by the total density of fermions. Additional experiments with the goal of reducing further the temperature are discussed in Ref. [12]. Thus, links to quantum chromodynamics (QCD) are possible [13], where dense cold matter with SU(3) color symmetry is created by the forces that confine quarks inside baryons and mesons through the exchange of SU(3) gauge bosons known as gluons. In particular, connections to color superconductivity in the absence of color-flip and color-orbit fields were made by several authors for continuum [14–16] and lattice [17] systems.

The relation between three-component ultracold fermions and color superconductivity in QCD is not only of academic interest, but also of experimental interest, as the gap between theoretical proposals and experimental realization closes due to technical advances. The type of color superfluidity in neutral ultracold fermions is expected to be related but somewhat different from the possibilities encountered in QCD, as quarks are electrically charged, have different masses, colors, and flavors, and thus color superconductivity of quarks is generically different [18–21]. For instance, it is quite difficult to realize in neutral ultracold fermions analogous phases to color flavor locking superconductivity [21–25], where three flavors are degenerate, because the number of internal degrees of freedom is very large. Even analogous phases to two-flavor superconductivity [18–21], where a preferred color pairing

channel is selected, are difficult to realize in the context of ultracold fermions. However, analogous phases to one-flavor superconductivity with three colors [26–28] are easier to realize in cold-atom systems, because one has to deal with only three internal states of the constitutive fermions.

Moreover, it has been suggested that color superconductivity of quark matter may occur naturally in compact neutron stars [29–31]. Since the higher-temperature regions of the QCD phase diagram are now being studied in heavy-ion collisions, it is important to use our knowledge of neutron star phenomena to understand if color superconductivity indeed appears in the high-density region of the QCD phase diagram. There have been even further suggestions that inhomogeneous color superconductivity phases emerge in neutron stars and are responsible for the glitches in rotational period of these compact stars [32]. Therefore, there has been observational interest in determining astrophysical consequences of color superconductivity.

Experiments involving color superconductivity in quark matter are not easy to perform, but tabletop experimental setups involving ultracold fermions with three internal states can serve as simulators of color superfluidity similar to color superconductivity in QCD. In addition, experiments with ultracold fermions with three internal states can also stand alone to serve as pointers for new directions and new phases of color superfluids that have no counterpart in QCD. A recent experimental development with a fermionic isotope of ytterbium (^{173}Yb) demonstrated that three internal states of the atom can be coupled to artificially created spin-orbit fields [33] via a Raman scheme with two counterpropagating lasers used earlier by Lin *et al.* in the context of a bosonic isotope of rubidium (^{87}Rb) with two internal states [34]. The interactions of ^{87}Rb cannot be adjusted, but it was possible to study the low-temperature phase diagram of ^{87}Rb in the presence of spin-orbit coupling and Zeeman fields both experimentally [34] and theoretically [35–37] for fixed interactions. Similar Raman schemes were used successfully in a fermionic isotope of potassium (^{40}K), where Fano-Feshbach resonances exist and interactions can be tuned in the presence of spin-orbit coupling for two internal states [38,39]. These experimental efforts on ^{40}K were developed concomitantly with various theoretical proposals [40–47] of spin-orbit-coupled fermions with two internal states, where interactions can be changed. Although experiments involving fermions in the Raman scheme are still performed at high temperatures ($T \approx 0.3E_F$), methods of reducing the temperature and of creating artificial spin-orbit or color-orbit fields in the laboratory are sought [48] using radio-frequency chip technology [49].

Thus, in this paper, we describe theoretically the possibility of color superfluidity in the presence of color-orbit and color-flip fields for trapped fermionic isotopes of lithium (^{6}Li), potassium (^{40}K), or ytterbium (^{173}Yb) with three internal states, to which we assign the color indices red (R), green (G), and blue (B). The remainder of the paper is organized as follows. In Sec. II we discuss in detail the independent-particle Hamiltonian and its spectrum, as well as the interaction terms between fermions of different colors. We also introduce the mixed-color representation that diagonalizes the independent-particle Hamiltonian, which is used later in Sec. IV to clarify the origin of various color superfluid phases. In Sec. III we discuss the emergence of color superfluidity in the presence of color-orbit and color-flip fields, within the saddle-point approximation at low temperatures. We solve the self-consistent equations for the order parameter tensor and particle number and obtain the low-temperature phase diagram in the space of color-flip versus interaction parameters, for fixed color-orbit coupling. Due to the presence of color-orbit coupling and color-flip fields, a set of five color superfluid phases emerges, with characteristic nodal structures in their excitation spectrum. These phases have a topological structure similar to Lifshitz transitions in metals under high pressure [50], but arise only due to the simultaneous presence of color-orbit coupling, color-flip fields, and interactions. Where five nodal color superfluid phases merge, we identify a quintuple point that is also pentacritical, given that the transition between superfluid phases is continuous. We also show that the low-temperature transitions between normal and color superfluid phases are continuous when color-orbit coupling is present and are discontinuous when color-orbit coupling is absent. In Sec. IV we describe the Hamiltonian in the mixed-color basis to make evident the emergence of the momentum dependence of the order parameter tensor and to shine light on the physical origin of the nodal structure of the quasiparticle and quasihole excitation spectrum. Furthermore, we also write the order parameter tensor in a total pseudospin basis to show that pairing can occur in singlet, triplet, and quintet sectors and to make comparisons with the case of spin-1/2 fermions, where only the singlet and triplet channels exist. In Sec. V we analyze the quasiparticle and quasihole excitation spectra in the mixed-color basis and show how the nodal structure and gaps emerge in the elementary excitation spectrum. Furthermore, we compute the momentum distributions for different colored fermions in various quantum phases to show how this easily measurable quantity can be used to identify different normal and superfluid phases. We also compute the density of states of colored fermions and show how they change as different normal and superfluid phases are visited in the phase diagram. In Sec. VI we discuss the applicability and limitations of the current work and comment on the role of Efimov states at lower particle densities, the possible emergence of nonuniform color superfluidity over a narrow region of the phase diagram, and the effects of fluctuations near the critical temperature between normal and color superfluid states. In Sec. VII we summarize our conclusions.

II. HAMILTONIAN

In order to describe interacting three-component fermions labeled by color states red (R), green (G), and blue (B), under the influence of color-orbit and color-flip fields, we begin with the most general independent-particle Hamiltonian resulting from suitably designed radio-frequency chip or Raman beams in the rotating frame

$$\mathbf{H}_0(\mathbf{k}) = \begin{pmatrix} \varepsilon_R(\mathbf{k}) & \Omega_{RG} & \Omega_{RB} \\ \Omega^*_{RG} & \varepsilon_G(\mathbf{k}) & \Omega_{GB} \\ \Omega^*_{GB} & \Omega^*_{GB} & \varepsilon_B(\mathbf{k}) \end{pmatrix}, \tag{1}$$

where $\varepsilon_c(\mathbf{k}) = (\mathbf{k} - \mathbf{k}_c)^2/2m + \eta_c$ represents the energy of internal state with color $c = \{R, G, B\}$ after a color-dependent net momentum transfer $\mathbf{k}_c$ provided by the Raman beams or

by the radio-frequency chip. Here η_c is a color-dependent reference energy of the atom in color state c. The matrix elements $\Omega_{cc'}$ represent a color-flip tensor (Rabi frequencies) that couples different atomic color states c and c'. We note in passing the use of units where Planck's and Boltzmann's constants are equal to one, that is, $\hbar = k_B = 1$.

We will be using throughout the paper the terminology *independent particle* instead of *single particle* when referring to Hamiltonians, energies, or other properties that describe a collection of a large number of particles that do not interact with each other. We follow the Feynman school of thought [51], where the single-particle nomenclature is reserved to describe just an individual particle rather than a collection of noninteracting particles.

Instead of analyzing the most general theoretical case shown in Eq. (1), we explore the simplest nontrivial experimental configuration, where the component Ω_{RB} of the color-flip tensor is zero, indicating that there is no coupling between states R and B, that is, $\Omega_{RB} = 0$. In addition, we consider that the matrix elements that couple states R to G or G to B are real and equal, that is, $\Omega_{RG} = \Omega^*_{RG} = \Omega_{GB} = \Omega^*_{GB} = \Omega$. Furthermore, we choose a symmetric situation, where momentum transfers occur only to color states R and B, such that $\mathbf{k}_R = k_T\hat{\mathbf{x}}$, $\mathbf{k}_G = 0$, and $\mathbf{k}_B = -k_T\hat{\mathbf{x}}$, where k_T is the magnitude of the momentum transferred to the atom by photons. Finally, we can define an overall energy reference via the sum $\sum_c \eta_c = \eta$, leading to internal energies $\eta_R = -\delta$, $\eta_B = \eta$, and $\eta_G = +\delta$, where δ represents the detuning of the photon frequencies for transitions between color states. Thus, we discuss next the simplest experimentally relevant independent-particle Hamiltonian for color states with color-dependent momentum transfer and color-flip terms.

A. Independent-particle Hamiltonian

For the simplest experimental realization discussed above, the independent-particle Hamiltonian for three color states described in Eq. (1) becomes

$$\mathbf{H}_{\rm IP}(\mathbf{k}) = \varepsilon(\mathbf{k})\mathbf{1} - h_x(\mathbf{k})\mathbf{J}_x - h_z(\mathbf{k})\mathbf{J}_z + b_z\mathbf{J}_z^2, \qquad (2)$$

where $\mathbf{J}_\ell$, with $\ell = \{x,y,x\}$, are spin-1 angular momentum matrices, $\varepsilon(\mathbf{k}) = \mathbf{k}^2/2m + \eta$ is a reference kinetic energy which is identical for all color states, $h_x(\mathbf{k}) = -\sqrt{2}\Omega$ plays the role of a color-flip field (like a spin-flip Zeeman field for spins), and $h_z(\mathbf{k}) = 2k_Tk_x/2m + \delta$ plays the role of a momentum-dependent Zeeman field along the z axis. Notice that $h_z(\mathbf{k}) = 2k_Tk_x/2m + \delta$ has two components. The first one $2k_Tk_x/2m$ represents color-orbit coupling controlled by the momentum transfer magnitude k_T and the second one represents a color-shift field controlled by the detuning δ (like a Zeeman shift for spins). Notice that $h_z(\mathbf{k})$ is transverse to the momentum transfer direction (x axis). Finally, the term $b_z = k_T^2/2m - \eta$ is a quadratic color shift (quadratic Zeeman shift) associated with the momentum transfer along the x direction.

To make further connections to QCD, we note that the independent-particle Hamiltonian described in Eq. (2) in general does not commute with the Gell-Mann matrices $\boldsymbol{\lambda}_j$, which are the eight generators of SU(3). To see this explicitly, it is sufficient to recall that the angular momentum matrices $\mathbf{J}_\ell$ can be written in terms of $\boldsymbol{\lambda}_j$ as $\mathbf{J}_x = (\boldsymbol{\lambda}_1 + \boldsymbol{\lambda}_6)/\sqrt{2}$ along the x direction, $\mathbf{J}_y = (\boldsymbol{\lambda}_2 + \boldsymbol{\lambda}_7)/\sqrt{2}$ along the y direction, and $\mathbf{J}_z = (\boldsymbol{\lambda}_3 + \sqrt{3}\boldsymbol{\lambda}_8)/2$ along the z direction and to show that the commutator $[\mathbf{H}_{\rm IP}, \boldsymbol{\lambda}_j] \neq 0$. The Hamiltonian above becomes SU(3) invariant only when the coefficients $h_x(\mathbf{k}) = h_z(\mathbf{k}) = b_z = 0$, rendering $\mathbf{H}_{\rm IP}(\mathbf{k})$ diagonal and proportional to the unit matrix $\mathbf{1}$, that is, all color states become degenerate.

A very similar independent-particle Hamiltonian was created in the laboratory for spin-1 bosonic ^{87}Rb atoms [52], where magnetic phases were investigated. Here, however, the independent-particle Hamiltonian corresponds to colored fermions, with potential candidates being ^{6}Li, ^{40}K, and ^{173}Yb. Thus, the independent-particle Hamiltonian matrix of Eq. (2) takes the explicit matrix form

$$\mathbf{H}_{\rm IP}(\mathbf{k}) = \begin{pmatrix} \varepsilon_R(\mathbf{k}) & -h_x(\mathbf{k})/\sqrt{2} & 0 \\ -h_x(\mathbf{k})/\sqrt{2} & \varepsilon_G(\mathbf{k}) & -h_x(\mathbf{k})/\sqrt{2} \\ 0 & -h_x(\mathbf{k})/\sqrt{2} & \varepsilon_B(\mathbf{k}) \end{pmatrix}, \qquad (3)$$

where the function $\varepsilon_R(\mathbf{k}) = \varepsilon(\mathbf{k}) - h_z(\mathbf{k}) + b_z$ represents the diagonal matrix element for the red (R) fermion, the function $\varepsilon_G(\mathbf{k}) = \varepsilon(\mathbf{k})$ represents the diagonal matrix element for the green (G) fermion, and the function $\varepsilon_B(\mathbf{k}) = \varepsilon(\mathbf{k}) + h_z(\mathbf{k}) + b_z$ represents the diagonal matrix element for the blue (B) fermion,

In second-quantized notation, the independent-particle Hamiltonian is

$$\hat{H}_{\rm IP} = \sum_{\mathbf{k}} \mathbf{F}^\dagger(\mathbf{k})\mathbf{H}_{\rm IP}(\mathbf{k})\mathbf{F}(\mathbf{k}), \qquad (4)$$

where the spinor operator is $\mathbf{F}^\dagger(\mathbf{k}) = [f_R^\dagger(\mathbf{k}), f_G^\dagger(\mathbf{k}), f_B^\dagger(\mathbf{k})]$, with $f_c^\dagger(\mathbf{k})$ creating a fermion with momentum $\mathbf{k} - \mathbf{k}_c$ in internal color state $c = \{R,G,B\}$. In order to bring the independent-particle Hamiltonian matrix into a diagonal form, we introduce next a mixed-color representation.

B. Mixed-color representation

The Hamiltonian matrix $\mathbf{H}_{\rm IP}(\mathbf{k})$ is diagonalized via the rotation $\Phi(\mathbf{k}) = \mathbf{R}(\mathbf{k})\mathbf{F}(\mathbf{k})$, where the rotation matrix $\mathbf{R}(\mathbf{k})$ satisfies the unitarity condition $\mathbf{R}^\dagger(\mathbf{k})\mathbf{R}(\mathbf{k}) = \mathbf{1}$. The spinor $\Phi(\mathbf{k})$ represents the basis of independent-particle eigenstates, whose elements are expressed as linear combinations of the elements of spinor $\mathbf{F}(\mathbf{k})$ in the original color basis via the rotation matrix

$$\mathbf{R}(\mathbf{k}) = \begin{pmatrix} R_{\Uparrow R}(\mathbf{k}) & R_{\Uparrow G}(\mathbf{k}) & R_{\Uparrow B}(\mathbf{k}) \\ R_{0R}(\mathbf{k}) & R_{0G}(\mathbf{k}) & R_{0B}(\mathbf{k}) \\ R_{\Downarrow R}(\mathbf{k}) & R_{\Downarrow G}(\mathbf{k}) & R_{\Downarrow B}(\mathbf{k}) \end{pmatrix}, \qquad (5)$$

where the normalization condition $\sum_c |R_{\alpha c}(\mathbf{k})|^2 = 1$ for each row guarantees the unitarity of $\mathbf{R}(\mathbf{k})$.

In this case, the independent-particle Hamiltonian becomes

$$\hat{H}_{\rm IP} = \sum_{\mathbf{k}} \Phi^\dagger(\mathbf{k})\mathbf{H}_M(\mathbf{k})\Phi(\mathbf{k}), \qquad (6)$$

where the spinor representing the diagonal basis is $\Phi^\dagger(\mathbf{k}) = [\phi_\Uparrow^\dagger(\mathbf{k}), \phi_0^\dagger(\mathbf{k}), \phi_\Downarrow^\dagger(\mathbf{k})]$, with $\phi_\alpha^\dagger(\mathbf{k})$ being the creation operator of a fermion with eigenenergy $\mathcal{E}_\alpha(\mathbf{k})$ and mixed-color label

$\alpha = \{\Uparrow, 0, \Downarrow\}$. The Hamiltonian matrix in diagonal form is

$$\mathbf{H}_M(\mathbf{k}) = \mathbf{R}(\mathbf{k})\mathbf{H}_{\rm IP}(\mathbf{k})\mathbf{R}^\dagger(\mathbf{k}) \tag{7}$$

with matrix elements $[\mathbf{H}_M]_{\alpha\beta}(\mathbf{k}) = \mathcal{E}_\alpha(\mathbf{k})\delta_{\alpha\beta}$, where $\mathcal{E}_\alpha(\mathbf{k})$ are the eigenvalues of the matrix $\mathbf{H}_{\rm IP}(\mathbf{k})$ shown in Eqs. (2) and (3). Finally, the independent-particle Hamiltonian in the mixed-color basis is simply written as

$$\hat{H}_{\rm IP} = \sum_{\mathbf{k}} \mathcal{E}_\alpha(\mathbf{k})\phi^\dagger_\alpha(\mathbf{k})\phi_\alpha(\mathbf{k}), \tag{8}$$

where the mixed-color operator $\phi_\alpha(\mathbf{k})$ is written as a linear combination of the color operators $f_c(\mathbf{k})$ via the matrix elements $R_{\alpha c}(\mathbf{k})$, that is, $\phi_\alpha(\mathbf{k}) = \sum_c R_{\alpha c}(\mathbf{k}) f_c(\mathbf{k})$. This is the general structure of eigenenergies and eigenstates of a system of independent colored particles in the presence of color-flip and color-orbit fields. Next we discuss a couple of simple limits and a specific example of this eigensystem.

C. Independent-particle spectrum

We discuss first the independent-particle eigenenergies in the limit where the quadratic color-shift term is zero, that is, $b_z = 0$ or $\eta = k_T^2/2m$, but the Rabi coupling $\Omega \neq 0$ and the detuning $\delta \neq 0$. In this situation, the eigenvalues of $\hat{H}_{\rm IP}$ have the simple form

$$\mathcal{E}_\alpha(\mathbf{k}) = \varepsilon(\mathbf{k}) - m_\alpha |h_{\rm eff}(\mathbf{k})|, \tag{9}$$

where the effective magnetic-field magnitude is $|h_{\rm eff}(\mathbf{k})| = \sqrt{h_x^2(\mathbf{k}) + h_z^2(\mathbf{k})}$ and $m_\Uparrow = +1, m_0 = 0$, and $m_\Downarrow = -1$. In this case, the independent-particle Hamiltonian $\hat{H}_{\rm IP}$ describes simply a pseudospin-1 system in the presence of the effective external field $\mathbf{h}_{\rm eff}(\mathbf{k}) = [h_x(\mathbf{k}), 0, h_z(\mathbf{k})]$.

A second simple limit of the more general color problem with $b_z \neq 0$, $\eta \neq 0$, $\Omega \neq 0$, and $\delta \neq 0$ discussed in Sec. II A corresponds to the case where $b_z = k_T^2/2m, \eta = 0, \Omega = 0$, and $\delta = 0$. In this situation the kinetic energies of the red, green, and blue states are, respectively, $\varepsilon_R(\mathbf{k}) = \varepsilon(\mathbf{k} - \mathbf{k}_T)$, $\varepsilon_G(\mathbf{k}) = \varepsilon(\mathbf{k})$, and $\varepsilon_B(\mathbf{k}) = \varepsilon(\mathbf{k} + \mathbf{k}_T)$, indicating that the blue states are shifted towards negative momenta along the x direction, while the red states are shifted towards positive momenta along the x direction, since $\mathbf{k}_T = k_T\hat{\mathbf{x}}$. In the limit where there is no color-orbit coupling, that is, $k_T = 0$, it is clear that the three kinetic energies are identical $\varepsilon_R(\mathbf{k}) = \varepsilon_G(\mathbf{k}) = \varepsilon_B(\mathbf{k}) = \varepsilon(\mathbf{k})$. These two situations are illustrated in Fig. 1.

From now on, in addition to setting $\eta = 0$ with $b_z = k_T^2/2m$, we will also set the detuning δ to zero, leading to $h_z(\mathbf{k}) = 2k_T k_x/2m$, but we keep the color-flip term $h_x(\mathbf{k}) = -\sqrt{2}\Omega$ with zero or nonzero Rabi frequencies Ω. This case is chosen to simplify the number of parameters involved, given that the problem of color superfluidity in the presence of color-orbit coupling and color-flip fields is sufficiently different, and thus there is no need to make matters more complex than they need to be. In passing, we mention that the case of finite detuning ($\delta \neq 0$) is also very rich given that parity is not conserved, thus affecting the normal state and superfluid phases that emerge, as well as their topological properties.

Throughout the paper, the energy scale that we use is the Fermi energy $E_F = k_F^2/2m$, where $k_F = (2\pi^2 n)^{1/3}$ is the Fermi momentum defined from total density of fermions $n = 3k_F^3/6\pi^2$, where the factor of 3 reflects the three colors

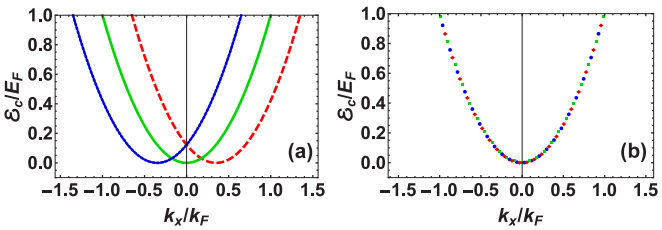

FIG. 1. Energy dispersions $\varepsilon_c(\mathbf{k})$ for red (R), green (G), and blue (B) states versus momentum along the k_x direction, for the parameters $b_z = k_T^2/2m$ ($\eta = 0$) and $\delta = 0$. The momentum transfer is (a) $k_T = 0.35k_F$ and (b) $k_T = 0$. The dashed red curve describes the R states, the solid green curve describes the G states, and the dotted blue curve describes the B states. Notice that the red dispersion is shifted to the right, the green dispersion has no shift, and the blue dispersion is shifted to the left when $k_T \neq 0$, but that all dispersions are identical when $k_T = 0$.

$\{R, G, B\}$. The same kinetic energies $\varepsilon(\mathbf{k}) = \mathbf{k}^2/2m$ are used here for all internal color states, since our momentum (k_F) and energy (E_F) units are fixed by setting the parameters η, k_T, Ω, and δ equal to zero.

In Fig. 2 we show plots of eigenvalues $\mathcal{E}_\alpha(\mathbf{k})$ versus momentum (k_x, k_y) with $k_z = 0$, for fixed momentum transfer $k_T = 0.35k_F$, zero detuning $\delta = 0$, and quadratic color-shift $b_z = k_T^2/2m$ ($\eta = 0$). In Fig. 2(a) we show the case where the color-flip term is small ($\Omega = 0.01E_F$) where single, double, and triple minima are shown in the upper, middle, and lower eigenenergies, respectively. In Fig. 2(b) we show the case where the Rabi frequency (color-flip term) is sufficiently large $\Omega = 0.2E_F$ such that the upper, middle, and lower eigenenergies have only a single minimum. The presence of color-orbit ($k_T \neq 0$) and color-flip ($\Omega \neq 0$) fields lifts the degeneracy of the color states $\{R, G, B\}$, which are assumed to have the same dispersion $\varepsilon(\mathbf{k}) = \mathbf{k}^2/2m$ when $k_T = 0, \Omega = 0$, and $\eta = 0$. For a fixed color-orbit coupling $k_T = \gamma k_F$, we can estimate when the three minima in the lower mixed-color band disappear by comparing the energy of the crossing point between the red and green or green and blue energy dispersions. The crossing points occur at momenta $k_x = \pm k_T/2 = \pm(\gamma/2)k_F$, so when $\Omega \sim (k_T/2)^2/2m = (\gamma^2/4)E_F$, the three minima of the lowest mixed-color band coalesce into one. The two minima in the

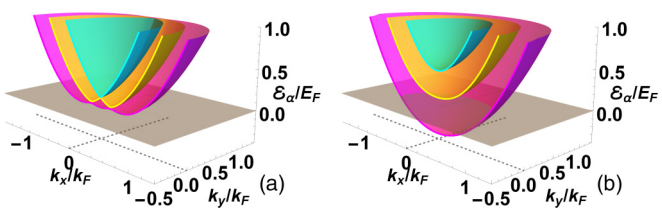

FIG. 2. Three-dimensional plots of the mixed-color eigenvalues $\mathcal{E}_\alpha(\mathbf{k})$ versus (k_x, k_y) with $k_z = 0$, when the quadratic color shift is $b_z = k_T^2/2m$ ($\eta = 0$) and the color-orbit coupling momentum transfer is $k_T = 0.35k_F$. (a) The color-flip field is $\Omega = 0.01E_F$, where the lower band (magenta) has three minima, the middle band (yellow) has two minima, and the upped band (cyan) has one minimum. (b) The color-flip field is $\Omega = 0.2E_F$, where all three bands (lower, middle, upper) have a single minimum.

middle mixed-color band become a single one, when the color-flip field Ω is of the order of the energy difference between the crossing points between red-blue bands and red-green or green-blue bands, that is, when $\Omega \sim k_T^2/2m - (k_T/2)^2/2m = (3\gamma^2/4)E_F$. For the specific case of $k_T = 0.35k_F$, the three minima of the lowest mixed-color band disappear when $\Omega \sim 0.03E_F$ and the two minima of the middle mixed-color band disappear when $\Omega \sim 0.09E_F$; therefore, in Fig. 2(b), where $\Omega = 0.2E_F$, each one of the three mixed-color bands has a single minimum.

Now that we have analyzed the independent-particle Hamiltonian for three-color fermions in the presence of color-orbit and color-flip fields, we are ready to discuss next the effects of interactions.

D. Interaction Hamiltonian

We begin our discussion of the effects of interactions between different color states in cold atoms by recalling that gluons are the mediators of quark-quark interactions in the color superconductivity problem encountered in QCD. Therefore, due to their dynamical nature, the interactions between quarks have a finite-range contribution and cannot be assumed to be of zero range. However, the situation encountered in cold atoms is simpler than in QCD, because the atomic fermions interact essentially via zero-range forces.

The interactions between different color states of cold fermions are essentially zero range and attractive $-g_{cc'}\delta(\mathbf{r}-\mathbf{r}')$ of strength $g_{cc'} > 0$, between internal states with different colors only, that is, $c \neq c'$. The use of contact (zero-range) interactions really means that the interaction range $R_{cc'}$ is much smaller than the interparticle distance k_F^{-1}, which is indeed the situation encountered experimentally in ultracold fermions, since these atoms are neutral.

Experimentally, interactions between atoms in different color (internal) states occur predominantly in the s-wave channel at low temperatures. Thus, we consider only interactions between the red-green (g_{RG}), red-blue (g_{RB}), and green-blue (g_{GB}) states to be nonzero, while all the red-red, green-green, and blue-blue interactions are negligible, that is, $g_{RR} = g_{GG} = g_{BB} = 0$. However, within the set of s-wave interactions, we could still have different interaction parameters, that is, $g_{RG} \neq g_{RB} \neq g_{GB}$. The zero-range nature of the interactions between colored fermions allows us to describe our system in terms of s-wave scattering lengths $a_{s,cc'}$ between different colors, as we will see later.

In momentum coordinates, the interaction part of the Hamiltonian has the structure

$$\hat{H}_{\rm int} = -\frac{1}{V}\sum_{\mathbf{Q},\{c\neq c'\}} g_{cc'}a^\dagger_{cc'}(\mathbf{Q})a_{cc'}(\mathbf{Q}), \tag{10}$$

where the volume of space is V and the paired-color creation operators are $a^\dagger_{cc'}(\mathbf{Q}) = \sum_{\mathbf{k}} f^\dagger_c(\mathbf{k}+\mathbf{Q}/2)f^\dagger_{c'}(-\mathbf{k}-\mathbf{Q}/2)$, with their center-of-mass momentum being $\mathbf{Q}$. Here the operators $f^\dagger_c(\mathbf{K})$ represent the creation of a fermion with color $c = \{R,G,B\}$ and momentum $\mathbf{K}$. As we will see soon, the expectation values of the operator $a^\dagger_{cc'}(\mathbf{Q})$ in a superfluid state describe the emergence of Cooper pairs in the BCS regime and of tightly bound pairs in BEC limit at low temperatures. We note in passing that $g_{cc'}$ has dimensions of energy times volume.

Having analyzed the interactions between different colored fermions, we will discuss next the full Hamiltonian, including the addition of the chemical potential to describe thermodynamic states with a fixed average number of particles.

E. Full Hamiltonian

The full Hamiltonian for a color superfluid with color-orbit coupling, color-flip fields, and contact interactions is

$$\hat{H} = \hat{H}_{\rm IP} + \hat{H}_{\rm int} - \mu\hat{N}, \tag{11}$$

with $\hat{N} = \sum_{c,\mathbf{k}} f^\dagger_c(\mathbf{k})f_c(\mathbf{k})$ representing the total number of colored fermions.

Having written the full Hamiltonian for the colored fermion problem with attractive interactions, we will discuss next the emergence of various color superfluid ground states, the nodal structure of their quasiparticle excitations, and the low-temperature phase diagram in the color-flip versus interaction parameter space for fixed color-orbit coupling.

III. SADDLE-POINT APPROXIMATION

In order to study the emergence of color superfluidity in the presence of color-flip and color-orbit fields, we focus here on superfluid phases of paired states with with zero center-of-mass momentum, that is, $\mathbf{Q} = \mathbf{0}$. Thus, the only relevant pairing operator is $a^\dagger_{cc'}(\mathbf{0}) = \sum_{\mathbf{k}} f^\dagger_c(\mathbf{k})f^\dagger_{c'}(-\mathbf{k})$. This implies that the emerging superfluid states are uniform throughout the sample volume, as it is discussed next, when we introduce the saddle-point approximation. This approximation is known to give excellent results at low temperatures as it captures both the emergence of large Cooper pairs in the BCS region and the emergence of tightly bound pairs (two-body bound states) in the BEC regime [53].

A. Order parameter and reduced Hamiltonian

Considering only pairing with zero center-of-mass momentum ($\mathbf{Q} = \mathbf{0}$), the order parameter for color superfluidity is defined by the tensor $\Delta_{cc'} = -g_{cc'}\langle a_{cc'}(\mathbf{0})\rangle/V$, with color indices $c \neq c'$ describing paired states RG, RB, and GB. Using a mean-field (saddle-point) approximation for the interaction term in Eq. (10) leads to the reduced Hamiltonian

$$\hat{H}_0 = \frac{1}{2}\sum_{\mathbf{k}} \mathbf{f}^\dagger_N(\mathbf{k})\mathbf{H}_0(\mathbf{k})\mathbf{f}_N(\mathbf{k}) + V\sum_{c\neq c'}\frac{|\Delta_{cc'}|^2}{g_{cc'}} + \mathcal{C}(\mu), \tag{12}$$

where the six-dimensional field operator $\mathbf{f}^\dagger_N(\mathbf{k}) = [f^\dagger_R(\mathbf{k}), f^\dagger_G(\mathbf{k}), f^\dagger_B(\mathbf{k}), f_R(-\mathbf{k}), f_G(-\mathbf{k}), f_B(-\mathbf{k})]$ represents a colored Nambu spinor, while the term $\mathcal{C}(\mu) = \frac{1}{2}\sum_{\mathbf{k}c}\xi_c(-\mathbf{k})$ contains the kinetic energy of colored fermions $\xi_c(\mathbf{k}) = \varepsilon_c(\mathbf{k}) - \mu$, which contributes to the ground-state energy.

The saddle-point Hamiltonian matrix is

$$\mathbf{H}_0(\mathbf{k}) = \begin{pmatrix} \overline{\mathbf{H}}_{\rm IP}(\mathbf{k}) & \mathbf{\Delta} \\ \mathbf{\Delta}^\dagger & -\overline{\mathbf{H}}^*_{\rm IP}(-\mathbf{k}) \end{pmatrix}, \tag{13}$$

where the 3×3 diagonal block matrix $\overline{\mathbf{H}}_{\rm IP}(\mathbf{k}) = \mathbf{H}_{\rm IP}(\mathbf{k}) - \mu\mathbf{1}$ represents the independent-particle Hamiltonian with respect

to the chemical potential μ and the 3×3 off-diagonal block matrix

$$\mathbf{\Delta} = \begin{pmatrix} 0 & \Delta_{RG} & \Delta_{RB} \\ -\Delta_{RG} & 0 & \Delta_{GB} \\ -\Delta_{RB} & -\Delta_{GB} & 0 \end{pmatrix} \tag{14}$$

represents the order parameter tensor $\Delta_{cc'}$, which is clearly antisymmetric since its transpose is equal to its negative $\Delta^T = -\Delta$ and thus traceless: $\mathrm{Tr}[\Delta] = 0$.

The quasiparticle and quasihole excitation spectrum can be found by diagonalizing the matrix shown in Eq. (13) or via the determinant $P(\omega) = \det[\omega\mathbf{1} - \mathbf{H}_0(\mathbf{k})]$. The characteristic polynomial $P(\omega) = \prod_j[\omega - E_j(\mathbf{k})]$ is of sixth degree; however, in the limit of zero detuning, where the color-shift field $\delta = 0$, we can use both quasiparticle-quasihole and parity symmetries to reduce $P(\omega)$ to the bicubic polynomial $P(\omega) = [\omega^2 - E_1^2(\mathbf{k})][\omega^2 - E_2^2(\mathbf{k})][\omega^2 - E_3^2(\mathbf{k})]$, which can be solved analytically using Cardano's method [54]. We show explicit solutions for $E_j(\mathbf{k})$ in Sec. V, but we warn the reader that the analytic solutions are not particularly illuminating.

In general, the six energy eigenvalues can be ordered as $E_1(\mathbf{k}) > E_2(\mathbf{k}) > E_3(\mathbf{k}) > E_4(\mathbf{k}) > E_5(\mathbf{k}) > E_6(\mathbf{k})$ and exhibit quasiparticle-quasihole symmetry in momentum space for any chosen value of the color-flip field (Rabi frequency) Ω or color-shift field (detuning) δ. In this case, we can choose quasiparticle-quasihole partners as follows: $E_6(\mathbf{k}) = -E_1(-\mathbf{k})$, $E_5(\mathbf{k}) = -E_2(-\mathbf{k})$, and $E_4(\mathbf{k}) = -E_3(-\mathbf{k})$. However, each eigenenergy $E_j(\mathbf{k})$ has well-defined parity only when the color-shift field (detuning) is zero, that is, $\delta = 0$, in which case $E_j(\mathbf{k}) = E_j(-\mathbf{k})$ is an even function of momentum $\mathbf{k}$.

Since the excitation spectrum $E_j(\mathbf{k})$ depends explicitly on the order parameter tensor $\Delta_{cc'}$ and the chemical potential μ, we establish next self-consistency relations for both quantities at fixed total density of colored fermions.

B. Self-consistency equations

The excitation spectrum $E_j(\mathbf{k})$ is determined by solving for the values of the order parameter amplitudes Δ_{RG}, Δ_{RB}, and Δ_{GB} and the chemical potential μ self-consistently. Starting from the thermodynamic potential $\mathcal{Q}_0 = -T\ln\mathcal{Z}$, where $\mathcal{Z} = \int\prod_c D[f_c^\dagger(\mathbf{k}), f_c(\mathbf{k})]\exp[-S]$ is the grand-canonical partition function and S is the action, we obtain the saddle-point action to be

$$TS_0 = -\frac{1}{2}\sum_{n,\mathbf{k}}\mathbf{f}_N^\dagger(\mathbf{k})\mathbf{G}^{-1}\mathbf{f}_N(\mathbf{k}) + V\sum_{c\neq c'}\frac{|\Delta_{cc'}|^2}{g_{cc'}} + \mathcal{C}(\mu),$$

where $\mathbf{G}^{-1}(i\omega_n,\mathbf{k}) = [i\omega_n\mathbf{1} - \mathbf{H}_0(\mathbf{k})]$ is the inverse of the resolvent (Green's) matrix $\mathbf{G}(i\omega_n,\mathbf{k})$. Here $\omega_n = (2n+1)\pi T$ is the fermionic Matsubara frequency and T is the temperature. Integration over the fermionic fields gives the saddle-point thermodynamic potential $\mathcal{Q}_0 = \mathcal{A}_0 + \mathcal{C}(\mu)$, with

$$\mathcal{A}_0 = -\frac{T}{2}\sum_{\mathbf{k}}\sum_{j=1}^{3}\ln\left\{2 + 2\cosh\left[\frac{E_j(\mathbf{k})}{T}\right]\right\} + V\sum_{c\neq c'}\frac{|\Delta_{cc'}|^2}{g_{cc'}}, \tag{15}$$

where the sum over the index j is over quasiparticles only, that is, $j = \{1,2,3\}$, given that we used the quasiparticle-quasihole symmetry described above.

Minimizing $\mathcal{Q}_0$ with respect to $\Delta_{cc'}^*$ via the condition $\delta\mathcal{Q}_0/\delta\Delta_{cc'}^* = 0$ leads to three order parameter equations

$$\frac{V}{g_{cc'}}\Delta_{cc'} = \frac{1}{2}\sum_{\mathbf{k}}\sum_{j=1}^{3}\tanh\left(\frac{\beta E_j(\mathbf{k})}{2}\right)\frac{\partial E_j(\mathbf{k})}{\partial\Delta_{cc'}^*} \tag{16}$$

for the available choices of $\Delta_{cc'} = \{\Delta_{RG},\Delta_{RB},\Delta_{GB}\}$ since $c \neq c'$. The total number of particles is fixed via the thermodynamic relation $N = -\partial\mathcal{Q}_0/\partial\mu|_{T,V}$, leading to the number equation

$$N = \frac{1}{2}\sum_{\mathbf{k}}\left[\sum_{j=1}^{3}\tanh\left(\frac{\beta E_j(\mathbf{k})}{2}\right)\frac{\partial E_j(\mathbf{k})}{\partial\mu} + 3\right]. \tag{17}$$

In the current problem, we can only fix the total number of colored fermions, because for an arbitrarily small color-flip field Ω the number operator $\hat{N}_c = \sum_{\mathbf{k}} f_c^\dagger(\mathbf{k})f_c(\mathbf{k})$ for a given color c does not commute with the full Hamiltonian $\hat{H}$ described in Eq. (11). For instance, the commutator of the independent-particle Hamiltonian $\hat{H}_{\mathrm{IP}}$ and the color number operator $\hat{N}_m$ for color m is $[\hat{H}_{\mathrm{IP}},\hat{N}_m] = \sum_{\mathbf{k},c}\{[\mathbf{H}_{\mathrm{IP}}]_{mc}f_c^\dagger(\mathbf{k})f_m(\mathbf{k}) - [\mathbf{H}_{\mathrm{IP}}]_{cm}f_m^\dagger(\mathbf{k})f_c(\mathbf{k})\}$, which only vanishes if the matrix $\mathbf{H}_{\mathrm{IP}}$ is diagonal, that is, when the color-flip field that causes transitions between different color states is zero: $h_x(\mathbf{k}) = 0$ (or $\Omega = 0$).

Before solving the self-consistency equations derived above, we use the generalized Lippmann-Schwinger relation $V/g_{cc'} = -mV/4\pi a_{s,cc'} + \sum_{\mathbf{k}}[\varepsilon_c(\mathbf{k}) + \varepsilon_{c'}(\mathbf{k})]^{-1}$ to express the bare coupling constant $g_{cc'}$ in terms of the scattering length $a_{s,cc'}$ in the absence of the color-orbit and color-flip fields, where we assume that the masses and the energy dispersions of all colored fermions are the same, that is, in this expression we take explicitly $\varepsilon_c(\mathbf{k}) = \varepsilon_{c'}(\mathbf{k}) = \mathbf{k}^2/2m$.

A more general case in the context of ultracold atoms corresponds to the situation where the interactions between different colors are not the same, that is, $g_{RG} \neq g_{RB} \neq g_{GB}$, which leads to different scattering lengths $a_{RG} \neq a_{RB} \neq a_{GB}$. This is indeed a more general situation, however, in fermionic isotopes of ytterbium [11,33], it is possible to select three internal atomic states such that the interactions are the same, that is, $g_{RG} = g_{RB} = g_{GB} = g$, which leads to $a_{RG} = a_{RB} = a_{GB} = a_s$, and to tune the scattering lengths via optical Feshbach resonances [55,56]. Such techniques may allow explorations of deep connections to SU(3) symmetric interactions in the context of color superconductivity of quark matter. Furthermore, when color-flip and color-orbit fields are considered in systems consisting of three internal states of fermionic isotopes of lithium, potassium, or ytterbium [57,58], even the simple limits of (a) single-channel interactions $g_{RG} = g_{GB} = 0$ and $g_{RB} \neq 0$ ($a_{RG} = a_{GB} = 0$ and $a_{RB} \neq 0$) can lead to color superfluidity [57] or (b) no interactions at all $g_{RG} = g_{GB} = g_{RB} = 0$ ($a_{RG} = a_{GB} = a_{RB} = 0$) can lead to nontrivial spinor physics [58].

In this work, we consider the case where s-wave interactions between different colors are exactly the same, that is, $g_{RG} = g_{GB} = g_{RB} = g$, but with $g_{RR} = g_{GG} = g_{BB} = 0$. In the absence of color-orbit ($k_T = 0$), color-flip ($\Omega = 0$), and

color-shift ($\delta = 0$) fields the three independent-particle bands corresponding to RGB states are identical; this implies that the pairing amplitudes between fermions of different colors are also identical, that is, $\Delta_{RG} = \Delta_{GB} = \Delta_{RB} = \Delta$, while $\Delta_{RR} = \Delta_{GG} = \Delta_{BB} = 0$. In this case, the order parameter tensor $\Delta_{cc'}$ is fully antisymmetric, but characterized by a single complex scalar Δ, which is independent of momentum $\mathbf{k}$. In such a situation, self-consistency is achieved via a single order parameter equation.

However, when color-orbit fields are present ($k_T \neq 0$), with zero color flip ($\Omega = 0$) and no color shift ($\delta = 0$), the three independent-particle bands are no longer identical (see Fig. 1), but under momentum inversion $\mathbf{k} \to -\mathbf{k}$ the red and blue bands are converted into each other, that is, $\varepsilon_R(\pm\mathbf{k}) = \varepsilon_B(\mp\mathbf{k})$, since $\varepsilon_R(\mathbf{k}) = \varepsilon(\mathbf{k} - \mathbf{k}_T)$ and $\varepsilon_B(\mathbf{k}) = \varepsilon(\mathbf{k} + \mathbf{k}_T)$, with $\varepsilon(\mathbf{k})$ being an even function of momentum $\mathbf{k}$. In this case, it is possible to have different uniform pairing amplitudes Δ_{RG}, Δ_{GB}, and Δ_{RB}, with the symmetry constraint that $\Delta_{RG} = \Delta_{GB} = \Delta_2$ and $\Delta_{RB} = \Delta_1$, while all the other pairing amplitudes continue to be zero, that is, $\Delta_{RR} = \Delta_{GG} = \Delta_{BB} = 0$. However, it is not required by symmetry that the order parameter amplitudes Δ_1 and Δ_2 are exactly the same. Similar considerations also apply to the independent-particle Hamiltonian shown in Eqs. (3) and (4) when color flip is present ($\Omega \neq 0$) with zero color shift ($\delta = 0$). In these cases, symmetry allows for different order parameter amplitudes Δ_1 and Δ_2 and two distinct order parameter equations (16).

The situation is even more complex when the color-shift field is not zero ($\delta \neq 0$). For instance, in the case where color orbit is present ($k_T \neq 0$) and color flip is absent ($\Omega = 0$), all three color bands are different, the energy dispersion for red fermions is $\varepsilon_R(\mathbf{k}) = \varepsilon(\mathbf{k} - \mathbf{k}_T) - \delta$, for green fermions it is $\varepsilon_G(\mathbf{k}) = \varepsilon(\mathbf{k})$, and for blue fermions it is $\varepsilon_B(\mathbf{k}) = \varepsilon(\mathbf{k} + \mathbf{k}_T) + \delta$. In this case, the pairing amplitudes Δ_{RG}, Δ_{GB}, and Δ_{RB} can all be distinct and determined by the self-consistent relations of Eq. (16).

In general, interactions can also be different $g_{RG} \neq g_{GB} \neq g_{RB}$ ($g_{RR} = g_{GG} = g_{BB} = 0$), leading automatically to non-identical order parameter components $\Delta_{RG} \neq \Delta_{GB} \neq \Delta_{RB}$ (with $\Delta_{RR} = \Delta_{GG} = \Delta_{BB} = 0$) even in the case of identical bands with zero color-orbit ($k_T = 0$), color-flip $\Omega = 0$, and color-shift ($\delta = 0$) parameters. Therefore, the three distinct order parameter equations described in Eq. (16) may be necessary.

The order parameter amplitudes Δ_{RG}, Δ_{GB}, and Δ_{RB} can be regarded as variational parameters used to describe color superfluidity. In the case of identical s-wave interactions, the simplest variational (saddle-point) state that can be considered to describe color superfluidity of fermions with and without color-orbit and color-flip fields is that where $\Delta_{RG} = \Delta_{GB} = \Delta_{RB} = \Delta$ and $\Delta_{RR} = \Delta_{GG} = \Delta_{BB} = 0$. This saddle-point state captures substantial nontrivial effects, while reducing dramatically the complexity of the numerical problem. Since we are interested in gaining insight into color superfluidity of fermions in the presence of color-orbit and color-flip fields, we discuss the simplest possible variational state allowed by symmetry and leave the more complex cases mentioned above for future detailed work.

Therefore, in the remainder of this paper, we consider fermions with identical s-wave interactions with or without color-orbit and color-flip fields and discuss the simplest variational state corresponding to a color order parameter tensor $\Delta_{cc'}$ that is characterized by a single complex component Δ in all s-wave pairing channels of colors $\{c,c'\} = \{R,G,B\}$. However, even in the simplest scenario, as we will see in Sec. IV, the order parameter becomes a momentum-dependent tensor $\Delta_{\alpha\beta}(\mathbf{k})$ with unequal components in all mixed-color channels $\{\alpha,\beta\}$, reflecting the different interactions and momentum dependences that are induced by color-flip and color-orbit fields into the mixed-color representation of the Hamiltonian. This leads to the emergence of momentum dependences reflecting induced p-wave and f-wave components as well as singlet, triplet, and quintuplet sectors in the total pseudospin basis of the mixed-color description.

Before we present the phase diagram of colored fermions in the presence of color-orbit and color-flip fields, it is important to look first at the limit where both terms are zero, that is, $h_z(\mathbf{k}) = 0$ ($k_T = 0$ and $\delta = 0$) as well as $h_x(\mathbf{k}) = 0$ ($\Omega = 0$). This limit serves as a reference and is discussed next.

C. Zero color-flip and color-orbit coupling

In the limit where color-orbit and color-flip fields vanish the evolution of a color superfluid from the BCS to the BEC regime is relatively simple. The independent-particle Hamiltonian matrix $\mathbf{H}_{\rm IP}(\mathbf{k})$ defined in Eq. (3) simplifies dramatically, since $h_z(\mathbf{k}) = 0$ ($k_T = 0$ and $\delta = 0$) and $h_x(\mathbf{k}) = 0$ ($\Omega = 0$), making $\mathbf{H}_{\rm IP}(\mathbf{k})$ diagonal and proportional to the unit matrix $\mathbf{1}$, that is, $\mathbf{H}_{\rm IP}(\mathbf{k}) = \varepsilon(\mathbf{k})\mathbf{1}$, with $\varepsilon(\mathbf{k}) = \mathbf{k}^2/2m$. This simplification makes the full Hamiltonian $\hat{H}$ defined in Eq. (11) invariant under global U(3) rotations of the color states. This means that $\hat{H}$ commutes with the nine generators of U(3). Furthermore, it is possible to perform simultaneous global U(3) rotations in the independent-particle $\overline{\mathbf{H}}_{\rm IP}(\mathbf{k}) = \mathbf{H}_{\rm IP}(\mathbf{k}) - \mu\mathbf{1}$ and pairing $\mathbf{\Delta}$ sectors of the saddle-point Hamiltonian matrix (13) such that the U(3)-rotated order parameter matrix $\mathbf{\Delta}_{\rm U(3)}$ can be represented by a single complex scalar $\Delta_{\rm U(3)} = \Delta\sqrt{3}$, with only two nonvanishing matrix entries, namely, $[\mathbf{\Delta}_{\rm U(3)}]_{13} = \Delta\sqrt{3}$ and $[\mathbf{\Delta}_{\rm U(3)}]_{31} = -\Delta\sqrt{3}$.

In this limiting case, the quasiparticle spectrum is $E_1(\mathbf{k}) = E_2(\mathbf{k}) = \sqrt{\xi^2(\mathbf{k}) + 3|\Delta|^2}$ and $E_3(\mathbf{k}) = \xi(\mathbf{k})$, where $\xi(\mathbf{k}) = \mathbf{k}^2/2m - \mu$, corresponding to a fully gapped superfluid with two degenerate quasiparticle states and a third quasiparticle state which is passive, that is, it represents free noninteracting fermions. This occurs because of the underlying global U(3) symmetry, which allows rotations into a mixed-color state, where only two mixed colors are active in pairing, while the third one is passive. In this case, a standard BCS-BEC crossover occurs [16] similar to the standard case of two internal states [59], but with the added feature that the third passive band provides a Fermi surface when the chemical potential lies above its minimum and no Fermi surface when the chemical potential is below its minimum. This reference case is illustrated in the phase diagram shown in Fig. 3(b) when $\Omega/E_F = 0$.

However, when color-orbit and color-flip fields are present the explicit global U(3) symmetry of the full Hamiltonian $\hat{H}$ in Eq. (11) is broken and all colors are involved in pairing, producing a complex excitation spectrum that allows also for exotic gapless quantum phases and phase transitions

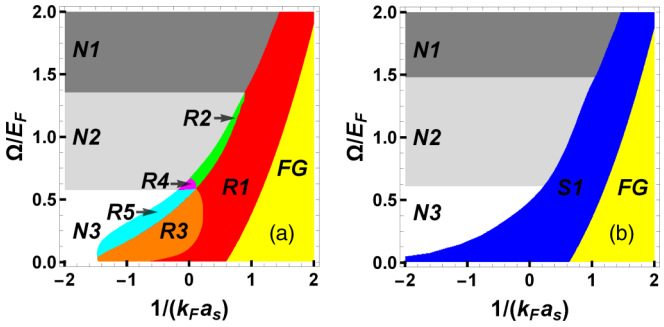

FIG. 3. Phase diagrams of the color-flip field Ω/E_F versus the scattering parameter $1/k_F a_s$ for a nonzero quadratic color shift $b_z = k_T^2/2m$ ($\eta = 0$) and two values of the color-orbit coupling controlled by momentum transfer k_T. The temperature is $T/E_F = 0.01$. In (a) $k_T = 0.35 k_F$ and the superfluid phases are labeled according to the nodal structure of the quasiparticle excitation spectrum that the color-orbit coupling induces when the Rabi field Ω/E_F is nonzero. The normal phases $N1$, $N2$, and $N3$ are labeled according to the number of Fermi surfaces they possess. The superfluid phases are labeled according to the number of nodal rings they possess ($R1$, $R2$, $R3$, $R4$, and $R5$). Phase transitions between various superfluid phases and between superfluid phases and normal states are continuous. In (b) $k_T = 0$ and the superfluid phases have either a fully nodal surface ($S1$) or a fully gapped (FG) phase. The fully nodal phase is reminiscent of the passive band when $\Omega = 0$, where only a crossover exist. The phase transition from the $S1$ phase to the normal phases is discontinuous.

between them, instead of a smooth crossover. These aspects are discussed next.

D. Low-temperature phase diagrams

When color-orbit and color-flip fields are present, the global U(3) symmetry is explicitly broken and there is no longer an inert mixed-color band. This means that all mixed-color bands participate in pairing and that the order parameter tensor in the mixed-color representation no longer has a single entry above the diagonal and a single entry below the diagonal. A detail analysis of the order parameter tensor in the mixed-color representation is performed in Sec. IV.

In order to obtain the phase diagram and classify the emergent superfluid and normal phases it is sufficient to analyze the quasiparticle-quasihole excitation spectrum $E_j(\mathbf{k})$, since all phases seen from the $\{R,G,B\}$ color basis have the same order parameter tensor $\Delta_{c,c'}$ and share the same color-symmetry controlled by a single complex component Δ. However, as the amplitude of Δ and chemical potential μ vary as a function of the color-flip field Ω/E_F and interactions $1/k_F a_s$ for fixed color-orbit fields, the nodal structure of the spectrum $E_j(\mathbf{k})$ suffers dramatic changes in momentum space and Lifshitz-like transitions occur in the superfluid states.

In Fig. 3 we show the phase diagrams of color superfluids in the color-flip field Ω/E_F versus the interaction parameter $1/k_F a_s$ plane. We consider only s-wave interactions between different colors and set the color-shift field to zero, that is, the detuning is set to zero $\delta = 0$ such that parity is preserved in the excitation spectrum. For Fig. 3(a) the parameters are $k_T = 0.35 k_F$ and $b_z = k_T^2/2m$ ($\eta = 0$) and for Fig. 3(b) the parameters are $k_T = 0$ and $b_z = k_T^2/2m$ ($\eta = 0$). The contrast between the two figures is remarkable, indicating that the presence of color-orbit and color-flip couplings induce novel superfluids states as interactions are changed. The phases $N1$, $N2$, and $N3$ correspond to the normal phases with one, two, and three Fermi surfaces associated with the eigenvalues of $\mathbf{H}_{\rm IP}(\mathbf{k})$ and characterize the regime where the colored Fermi gas is degenerate. The lines separating these normal phases correspond to simple Lifshitz transitions [50].

The superfluid phases in Fig. 3(a) are labeled according to their nodal structure, which in the present case corresponds to rings of zero-energy quasiparticles representing the residual Fermi surface of the starting degenerate colored Fermi gas. In the presence of color-orbit and color-flip fields, the quasiparticle excitation energies $E_1(\mathbf{k})$, $E_2(\mathbf{k})$, and $E_3(\mathbf{k})$ have more complex momentum dependence, but only $E_3(\mathbf{k})$ can have zeros. The zeros of $E_3(\mathbf{k})$ define the loci (points, lines, or surfaces) in momentum space, where there is no energy cost to create quasiparticle excitations. The connectivity of these loci of zero energy can be used to classify the topologically distinct superfluid phases of colored fermions.

To analyze the phase diagram, we make use of the mixed-color bands $\mathcal{E}_\alpha(\mathbf{k})$ with $\alpha = \{\Uparrow, 0, \Downarrow\}$, as discussed in Sec. II B. For definiteness, we fix first the color-flip coupling to $\Omega/E_F = 0.29$, in which case there are three mixed-color bands participating in pairing. As the scattering parameter $1/k_F a_s$ increases a nodal phase $R5$ with five rings, three in the outer $\Uparrow$, one the middle 0, and one in the inner $\Downarrow$ band, gives way to a nodal phase $R3$ with three rings in the outer $\Uparrow$ band, where the two internal rings annihilate at finite momenta in the $(0,k_y,k_z)$ plane. This leads to the opening of a gap at the $R5$-$R3$ boundary, but residual node lines persist. An additional increase of the scattering parameter leads to the one ring $R1$ phase in the outer $\Uparrow$ band, where the two other rings shrink to points at finite momenta along the $(k_x,0,0)$ direction when the phase boundary $R3$-$R1$ is reached. Finally, a further increase in the scattering parameter transforms the $R1$ phase into a fully gapped (FG) phase with no nodal regions. A similar analysis can be done for different fixed values of Ω/E_F and varying scattering parameter. An important observation is the existence of a quintuple point, where the five superfluid phases $R1$, $R2$, $R3$, $R4$, and $R5$ merge. The transitions between these topologically distinct superfluid phases are all continuous, therefore this quintuple point is also pentacritical. In Fig. 4 we plot the nodal structure of the $N3$, $R5$, $R3$, and $R1$ phases illustrated in the phase diagram of Fig. 3(a), for fixed value of $\Omega/E_F = 0.29$ and varying scattering parameter $1/k_F a_s$.

The richness of the phase diagram in Fig. 3(a) should be contrasted with simplicity of that in Fig. 3(b), where the color-orbit coupling parameter is set to zero, that is, $k_T = 0$. Indeed, in the case of Fig. 3(b) the phase diagram is much simpler. When the color-orbit and color-flip couplings are zero, that is, $k_T = 0$ and $\Omega = 0$, pairing occurs only between two mixed colors which produce a fully gapped superfluid, but the third mixed color is completely inert [16] and thus possesses the original Fermi surface for noninteracting fermions when the chemical potential lies above the minimum of the band. This situation corresponds to the line of $\Omega/E_F = 0$ in Fig. 3(b) and describes standard BCS-BEC crossover physics, where the superfluid is always gapped as a function the interaction parameter $1/k_F a_s$.

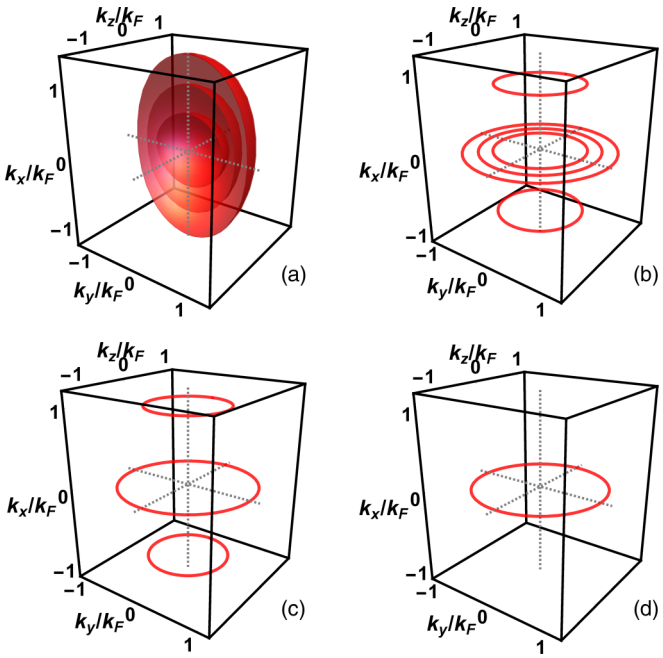

FIG. 4. Nodal structure of the quasiparticle excitation spectrum for phases $N3$, $R5$, $R3$, and $R1$ with the parameters $\Omega = 0.29E_F$, $k_T = 0.35k_F$, and $b_z = k_T^2/2m$ ($\eta = 0$): (a) normal phase $N3$ with three Fermi surfaces, where $1/k_F a_s = -1.31$, $\mu/E_F = 0.97$, and $|\Delta| = 0$; (b) five-ringed superfluid phase $R5$, where $1/k_F a_s = -1.03$, $\mu/E_F = 0.97$, and $|\Delta|/E_F = 0.0056$; (c) three-ringed superfluid phase $R3$, where $1/k_F a_s = -0.069$, $\mu/E_F = 0.81$, and $|\Delta|/E_F = 0.31$; and (d) one-ringed superfluid phase $R1$, where $1/k_F a_s = 0.62$, $\mu/E_F = 0.19$, and $|\Delta|/E_F = 0.73$.

However, when k_T is still zero, but the color-flip field Ω is nonzero, extra mixing of colors occur and the inert band becomes active. Nevertheless, a single nodal surface continues to exist, as illustrated in the blue ($S1$) region. For $\Omega/E_F \neq 0$, the quasiparticle dispersion $E_3(\mathbf{k})$ is no longer identical to the independent-particle energy $\xi(\mathbf{k})$ and the nodal structure of $E_3(\mathbf{k})$ is completely isotropic in momentum space. Thus, for finite Ω/E_F, there is a phase transition between a gapless superfluid with surface nodes ($S1$) to a FG superfluid phase. For fixed Ω/E_F, the line separating the $S1$ and FG phases appears when the degeneracy between the lowest-energy mixed-color band $\xi_{\Uparrow}(\mathbf{k}) = \mathcal{E}_{\Uparrow}(\mathbf{k}) - \mu$ and its counterpart $-\xi_{\Uparrow}(\mathbf{k})$ at $\xi_{\Uparrow}(\mathbf{k}) = 0$ is lifted by nonzero color-flip fields ($\Omega \neq 0$). This occurs when the chemical potential μ falls below the minimum value $\min_{\mathbf{k}}\{\mathcal{E}_{\Uparrow}(\mathbf{k})\}$, when a full gap in the excitation spectrum $E_3(\mathbf{k})$ emerges, leading to the yellow (FG) region in Fig. 3(b). The quasiparticle bands $E_1(\mathbf{k})$ and $E_2(\mathbf{k})$ are always gapped in the present case.

In addition, when color-orbit coupling is zero ($k_T = 0$), the transition from superfluid to normal phases is discontinuous (first order) at the low temperatures indicated in Fig. 3(b) and the phase boundary corresponds to the balancing of the color-flip (magnetic) energy $h_x \chi_{xx} h_x/2$, where χ_{xx} is the color-flip (magnetic) susceptibility and the condensation energy of the superfluid $\gamma|\Delta|^2$. This leads to $\Omega = |\Delta|\gamma/\chi_{xx}$ at the phase boundary, where the order parameter amplitude $|\Delta|$ jumps discontinuously to zero. Such a relation for color superfluids is a generalization of Clogston's result for Fermi superfluids paired with zero center-of-mass momentum in the singlet s-wave state of two spin-1/2 fermions [60].

Another important difference between phase diagrams illustrated in Figs. 3(a) and 3(b) concerns the limit when the color-flip field vanishes, that is, when $\Omega \to 0$. In Fig. 3(a) the color-orbit coupling is nonzero, that is, $k_T \neq 0$, meaning that the red-color (R) band is shifted to the left, the green-color (G) band remains in the same place, and the blue-color (B) band is shifted to the right, as shown in Fig. 1. Given that s-wave interactions only lead to RG, RB, and GB pairs, this implies that pairing with zero center-of-mass momentum for RB pairs can occur without energy cost, but pairing with zero center-of-mass momentum for RG and GB pairs costs energy of an amount $k_T^2/2m \pm k_x k_T/m$. Therefore, even for zero color-flip fields ($\Omega = 0$), a uniform zero center-of-mass superfluid phase is not favored until a critical value of the interaction parameter $1/k_F a_s$ is reached. This is in sharp contrast with the case of two internal states, where the spin-orbit coupling shifts one band to the right and the other to the left and does not affect zero center-of-mass momentum pairing. This occurs because of the existence of a spin-gauge symmetry, which can be used to gauge away the momentum transfer k_T from the problem when $\Omega = 0$. The corresponding color-gauge symmetry for the color superfluid problem is broken and thus a color-gauge symmetry does not exist even when $\Omega = 0$. This means that the cases of $\Omega = 0$ with $k_T = 0$ and with $k_T \neq 0$ are not equivalent. Furthermore, while in the two-state case uniform superfluidity is always present at zero temperature for any values of $\Omega \neq 0$ and $k_T \neq 0$ [46], in the color problem at hand this is not the case, because of the energy cost associated with pairing in the RG and GB channels, and thus normal states phases may be present at zero temperature.

Having discussed some general aspects of the phase diagram of color superfluids in the presence of color-orbit coupling and color-flip fields, we discuss next a few thermodynamic consequences involving the thermodynamic potential and the equation of state for the chemical potential.

E. Thermodynamic potential

In the vicinity of the phase transition between the normal and superfluid phases, the thermodynamic potential in the superfluid phase $\mathcal{Q}_0[\Delta, \Delta^*]$ can be expanded about the normal state value $\mathcal{Q}_N$ as

$$\mathcal{Q}_0 = \mathcal{Q}_N + a|\Delta|^2 + \frac{b}{2}|\Delta|^4 + \frac{c}{3}|\Delta|^6. \tag{18}$$

The coefficients a, b, c, and $\mathcal{Q}_N$ depend on the microscopic parameters of the theory such as the color-flip field Ω, the color-orbit momentum transfer k_T, and the scattering length a_s, as well as on thermodynamic parameters such as chemical potential μ and temperature T. The coefficient c is found to be always positive in the range of parameters investigated and that guarantees the stability of the Ginzburg-Landau expansion shown in Eq. (18).

In Fig. 5 all plots correspond to fixed temperature $T/E_F = 0.01$ and color-flip field $\Omega/E_F = 0.29$. In Figs. 5(a) and 5(b) we show the thermodynamic potential difference $\delta\mathcal{Q} = \mathcal{Q}_0 - \mathcal{Q}_N$ for two values of scattering parameter $1/k_F a_s$ slightly

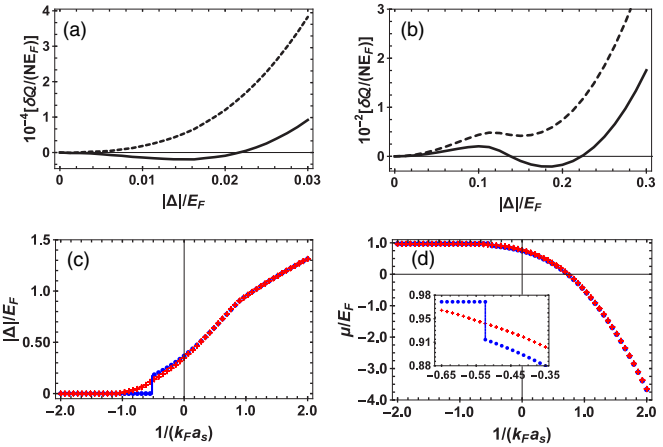

FIG. 5. (a) and (b) Difference $\delta\Omega$ between thermodynamic potentials of the superfluid Ω_0 and normal state Ω_N at $T/E_F = 0.01$ and $\Omega/E_F = 0.29$. In (a) $\delta\Omega$ is shown for $k_T/k_F = 0.35$ and the dashed line exhibits a global minimum at $|\Delta| = 0$ and describes the normal phase for the parameter values $1/k_F a_s = -1.17$ and $\mu/E_F = 0.97$. The solid line shows a global minimum at $|\Delta|/E_F = 0.015$ and describes a superfluid phase for the parameter values $1/k_F a_s = -0.97$ and $\mu/E_F = 0.97$. The transition from the superfluid to the normal state is continuous (second order). In (b) $\delta\Omega$ is shown for $k_T/k_F = 0$ and the dashed line shows a global minimum at $|\Delta| = 0$ and describes the normal phase for the parameter values $1/k_F a_s = -0.62$ and $\mu/E_F = 0.97$. The solid line shows a global minimum at $|\Delta|/E_F = 0.18$ and describes a superfluid phase for the parameter values $1/k_F a_s = -0.48$ and $\mu/E_F = 0.91$. In (c) and (d) the curves with blue circles describe the case of zero color-orbit coupling ($k_T = 0$) and the curves with red crosses describe the case with $k_T \neq 0$. (c) Order parameter amplitude $|\Delta|/E_F$ versus scattering parameter $1/k_F a_s$ for $T/E_F = 0.01$ and $\Omega/E_F = 0.29$. (d) Chemical potential μ/E_F versus scattering parameter $1/k_F a_s$ for $T/E_F = 0.01$ and $\Omega/E_F = 0.29$. Notice the discontinuous jumps in $|\Delta|/E_F$ and μ/E_F for the curves with blue circles at the transition from the superfluid to the normal state.

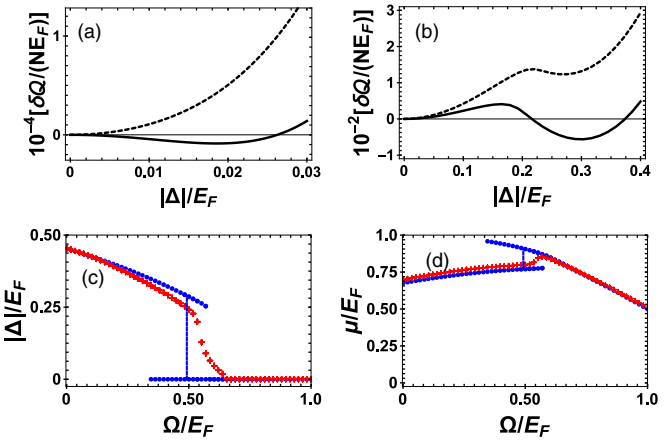

FIG. 6. Unitarity limit $1/k_F a_s = 0$ at temperature $T/E_F = 0.01$. (a) and (b) Difference $\delta\Omega$ between thermodynamic potentials of the superfluid Ω_0 and normal state Ω_N. In (a) the color-orbit coupling is $k_T = 0.35 k_F$, the solid line corresponds to the parameters $\Omega/E_F = 0.64$ and $\mu/E_F = 0.81$, and the dashed line corresponds to $\Omega/E_F = 0.67$ and $\mu/E_F = 0.79$. In (b) the color-orbit coupling is $k_T = 0$, the solid line corresponds to the parameters $\Omega/E_F = 0.47$ and $\mu/E_F = 0.77$, and the dashed line corresponds to $\Omega/E_F = 0.53$ and $\mu/E_F = 0.77$. In (c) and (d) the blue circles (red crosses) correspond to $k_T/k_F = 0$ ($k_T/k_F = 0.35$). (c) Order parameter amplitude $|\Delta|/E_F$ versus Ω/E_F. (d) Chemical potential μ/E_F versus Ω/E_F. The vertical blue solid lines indicate the locations of the discontinuous transitions and the end points of the lines of blue circles show the hysteretic behavior in $|\Delta|/E_F$ and μ/E_F due to the existence of a metastable minimum in the thermodynamic potential shown in (b).

before and after the transition from the normal to the superfluid state. The difference $\delta\Omega$ is shown in units of NE_F, where N is the total particle number. In Fig. 5(a) [Fig. 5(b)] the color-orbit coupling momentum transfer is $k_T/k_F = 0.35$ ($k_T/k_F = 0$) and the transition from the normal phase to the superfluid phase is continuous (discontinuous), according to Landau's classification, as can be seen from the plot of $\delta\Omega$ versus $|\Delta|/E_F$. For the range of parameters investigated at temperature $T/E_F = 0.01$, the phase transition between the normal and superfluid phase is always discontinuous for the case of $k_T = 0$ and is always continuous for the case of $k_T/k_F = 0.35$. The order parameter amplitude $|\Delta|/E_F$ versus scattering parameter $1/k_F a_s$ is shown in Fig. 5(c) for $k_T = 0$ and $k_T/k_F = 0.35$ and a clear discontinuity in $|\Delta|/E_F$ occurs at the normal-superfluid phase boundary when $k_T = 0$, while $|\Delta|/E_F$ reaches zero continuously when $k_T/k_F = 0.35$. In Fig. 5(d) we show the chemical potential μ/E_F for $k_T/k_F = 0$ and for $k_T/k_F = 0.35$. While for $k_T/k_F = 0.35$ the chemical potential μ/E_F evolves smoothly with scattering parameter $1/k_F a_s$, by contrast, there is a discontinuous jump in μ/E_F in the case of $k_T/k_F = 0$, as the phase boundary between the normal and superfluid states is crossed.

In order to investigate the existence of the Clogston limit, we analyze our system at the unitarity limit where the scattering parameter $1/k_F a_s = 0$ and describe changes in the thermodynamic potential, order parameter amplitude $|\Delta|/E_F$, and chemical potential μ/E_F versus the color-flip parameter Ω/E_F. In Fig. 6 we show the difference $\delta\Omega$ between thermodynamic potentials of the superfluid Ω_0 and normal state Ω_N.

The plots shown in Fig. 6 refer to the unitarity limit $1/k_F a_s = 0$ at temperatures $T/E_F = 0.01$. In Fig. 6(a) the thermodynamic potential difference $\delta\Omega$ is plotted for color-orbit coupling $k_T = 0.35 k_F$: The solid line corresponds to the parameters $\Omega/E_F = 0.64$ and $\mu/E_F = 0.81$, while the dashed line corresponds to $\Omega/E_F = 0.67$ and $\mu/E_F = 0.79$. In Fig. 6(b) $\delta\Omega$ is plotted for color-orbit coupling $k_T = 0$: The solid line corresponds to the parameters $\Omega/E_F = 0.47$ and $\mu/E_F = 0.77$, while the dashed line corresponds to $\Omega/E_F = 0.53$ and $\mu/E_F = 0.77$. In Figs. 6(c) and 6(d) the blue circles (red crosses) correspond to $k_T/k_F = 0$ ($k_T/k_F = 0.35$). In Fig. 6(c) the order parameter amplitude $|\Delta|/E_F$ versus Ω/E_F is shown and in Fig. 6(d) the chemical potential μ/E_F versus Ω/E_F is shown. Notice the hysteretic behavior characteristic of discontinuous (first-order) phase transitions when the color-orbit coupling is $k_T/k_F = 0$.

Two important effects are illustrated in the panels of Fig. 6. First, there is a well-defined Clogston limit when the color-orbit coupling $k_T/k_F = 0$, leading to a discontinuous (first-order) transition from superfluid to normal phases.

Second, when the color-orbit parameter $k_T/k_F \neq 0$, the standard Clogston limit is exceeded and the transition to the normal state becomes continuous (second order). The discontinuous phase transition from superfluid to normal phases for zero color-orbit coupling ($k_T/k_F = 0$) and finite color-flip field $\Omega \neq 0$ becomes continuous for arbitrarily small $k_T/k_F \ll 1$ and $\Omega \neq 0$, provided a uniform superfluid is the stable ground state. The discontinuity in the order parameter $|\Delta|/E_F$ at the phase boundary ceases to exist for arbitrarily small color-orbit coupling, suggesting that k_T/k_F is a microscopic parameter that controls the nonuniform convergence of $|\Delta|/E_F$ versus the scattering parameter $1/k_F a_s$ or versus the color-flip parameter Ω/E_F.

The nonuniform convergence of $|\Delta|/E_F$ is similar mathematically to the nonuniform convergence of the Fermi function, where only at zero temperature it develops a discontinuity as a function of momentum. In the present case, the physical origin of the nonuniform convergence is quite different. In our current problem, attractive interactions are assumed to occur only between different colors, such that pairing can only exist in the s-wave channel. Thus, in the strict case where color-orbit coupling is zero ($k_T/k_F = 0$) there is a cost in color-flip energy associated with pairing and thus there is a Clogston limit even in the color problem at low temperatures. However, when a uniform superfluid solution is the ground state for $k_T/k_F \neq 0$, then higher-order angular momentum pairing is induced by the color-orbit coupling as suggested by the nodal structures shown in Fig. 4. Thus, pairing in the mixed-color states may occur not only in the singlet channel, but also in the triplet or quintet channels. This allows the color superfluid to respond to a color-flip field by simply rotating the triplet or quintet mixed-color state without breaking pairs and thus beating the standard Clogston limit. An analysis of the order parameter in the mixed-color basis is therefore important for a deeper understanding of the phase diagram obtained in Fig. 3.

Now that we have analyzed a few thermodynamic properties of color superfluids and characterized the transitions between the normal and superfluid states, we are ready to investigate in detail the structure of the order parameter in each one of the superfluid phases found.

IV. HAMILTONIAN IN A MIXED-COLOR BASIS

In order to understand in more detail the different superfluid phases that emerge, it is important to analyze the microscopic Hamiltonian in a mixed-color basis that diagonalizes the independent-particle Hamiltonian discussed in Sec. II A.

The excitation spectrum and the momentum space topology of colored quasiparticles and quasiholes can be understood by writing the saddle-point Hamiltonian $\mathbf{H}_0(\mathbf{k})$ defined in Eq. (13) as

$$\widetilde{\mathbf{H}}_0(\mathbf{k}) = \begin{pmatrix} \mathbf{H_M}(\mathbf{k}) & \mathbf{\Delta}_M \\ \mathbf{\Delta}_M^\dagger & -\mathbf{H}_M^*(-\mathbf{k}) \end{pmatrix} \tag{19}$$

in the mixed-color basis. The matrix elements of $\mathbf{H}_M(\mathbf{k})$ represent the mixed-color energy bands and are given by $\mathbf{H}_{M,\alpha\beta}(\mathbf{k}) = \xi_\alpha(\mathbf{k})\delta_{\alpha\beta}$ with energies $\xi_\alpha(\mathbf{k}) = \mathcal{E}_\alpha(\mathbf{k}) - \mu$ measured with respect to the chemical potential μ, while the matrix elements of $\mathbf{\Delta}_M$ are $\Delta_{M,\alpha\beta}(\mathbf{k}) = \Delta_{\alpha\beta}(\mathbf{k})$, representing the order parameter tensor in the mixed-color basis labeled by indices $\{\alpha,\beta\} = \{\Uparrow, 0, \Downarrow\}$. The elements $\Delta_{\alpha\beta}(\mathbf{k})$ are strongly momentum *dependent*, in sharp contrast to the elements $\Delta_{cc'}(\mathbf{k})$ of the original matrix $\mathbf{\Delta}$, defined in Eq. (14), which are *independent* of momentum. In order to elucidate the symmetry properties of fermion pairs, we analyze next the order parameter tensor in the mixed-color basis.

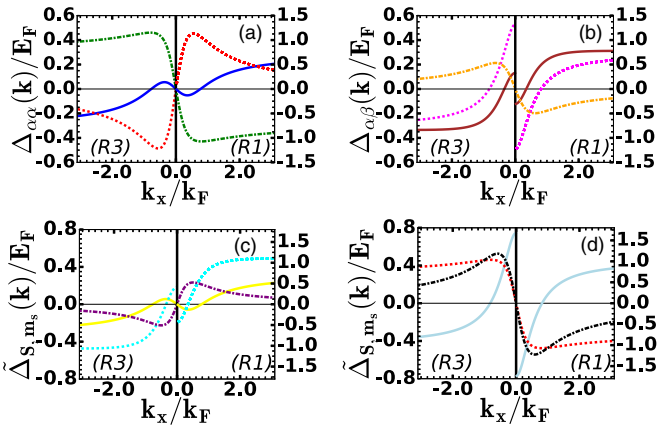

FIG. 7. Plots of the components of the order parameter tensors (a) and (b) $\Delta_{\alpha\beta}(\mathbf{k})$ and (c) and (d) $\widetilde{\Delta}_{Sm_s}(\mathbf{k})$ versus momentum $(k_x,0,0)$. We show plots for the $R3$ phase with the scattering parameter $1/k_F a_s = -0.07$ ($\mu/E_F = 0.81$ and $|\Delta|/E_F = 0.31$) corresponding to the vertical scale on the left. We also show plots for the $R1$ phase with the scattering parameter $1/k_F a_s = 0.62$ ($\mu/E_F = 0.19$ and $|\Delta|/E_F = 0.73$) corresponding to the vertical scale on the right. In (a) the solid blue curve describes $\Delta_{\Uparrow\Uparrow}(\mathbf{k})$, the dashed red curve describes $\Delta_{00}(\mathbf{k})$, and the dash-dotted green curve describes $\Delta_{\Downarrow\Downarrow}(\mathbf{k})$. In (b) the solid brown line represents $\Delta_{\Uparrow 0}(\mathbf{k})$, the dashed magenta line represents $\Delta_{\Downarrow 0}(\mathbf{k})$, and the dash-dotted orange line represents $\Delta_{\Uparrow\Downarrow}(\mathbf{k})$. In (c) the solid yellow curve corresponds to $\widetilde{\Delta}_{22}(\mathbf{k})$, the dashed cyan curve corresponds to $\widetilde{\Delta}_{21}(\mathbf{k})$, and the dash-dotted purple curve corresponds to $\widetilde{\Delta}_{20}(\mathbf{k})$. In (d) the solid light blue line indicates $\widetilde{\Delta}_{2\bar{1}}(\mathbf{k})$, the dashed red line indicates $\widetilde{\Delta}_{2\bar{2}}(\mathbf{k})$, and the dash-dotted black line indicates $\widetilde{\Delta}_{00}(\mathbf{k})$.

A. Order parameter in a mixed-color basis

The order parameter tensor in the mixed-color basis can be written as

$$\Delta_{\alpha\beta}(\mathbf{k}) = R_{\alpha c}(\mathbf{k})\Delta_{cc'}R_{c'\beta}(-\mathbf{k}), \tag{20}$$

where Einstein's summation convention of repeated indices is understood and the $R_{\alpha c}(\mathbf{k})$ are matrix elements of the color-mixing matrix $\mathbf{R}(\mathbf{k})$ in Eq. (5), where the α-row elements $\mathbf{R}_\alpha(\mathbf{k}) = [R_{\alpha R}(\mathbf{k}), R_{\alpha G}(\mathbf{k}), R_{\alpha B}(\mathbf{k})]$ are the eigenvectors of the independent-particle Hamiltonian matrix $\mathbf{H}_{\rm IP}(\mathbf{k})$. The order parameter matrix in the mixed-color basis has the property $\Delta_{\alpha\beta}(\mathbf{k}) = -\Delta_{\beta\alpha}(-\mathbf{k})$ due to Fermi statistics. Such a condition ensures that the diagonal elements $\Delta_{\alpha\alpha}(\mathbf{k})$ have odd parity, as required by the Pauli exclusion principle. However, in general, this is not sufficient to force the off-diagonal elements to have well-defined parity.

In Fig. 7 we describe in detail the momentum dependence of the order parameter tensor along $(k_x,0,0)$ in the

mixed-color basis [Figs. 7(a) and 7(b)] and in the total pseudospin basis [Figs. 7(c) and 7(d)] for the parameters $\Omega/E_F = 0.29$, $k_T/k_F = 0.35$, and $b_z = k_T^2/2m$ ($\eta = 0$). The order parameter tensor on either basis depends on momentum only along the k_x direction and is independent of momentum along k_y and k_z, due to the one-dimensional nature of the color-orbit coupling. In Figs. 7(a)–7(d) we show only two cases. The first one corresponds to the $R3$ phase with the scattering parameter $1/k_F a_s = -0.07$ ($\mu/E_F = 0.81$ and $|\Delta|/E_F = 0.31$) and the plots correspond to the vertical scale on the left. The second case corresponds to the $R1$ phase with the scattering parameter $1/k_F a_s = 0.62$ ($\mu/E_F = 0.19$ and $|\Delta|/E_F = 0.73$) and the plots correspond to the vertical scale on the right.

In Fig. 7(a) we show the momentum dependence of the diagonal components $\Delta_{\alpha\alpha}(\mathbf{k})$ of the order parameter tensor in two cases. From these plots it is evident that the nodal structure of the order parameter tensor components $\Delta_{\alpha\alpha}(\mathbf{k})$ is exactly the same for the $R3$ and $R1$ phases. The only difference between the two cases is the overall magnitude of the amplitude $|\Delta|$ reflected in the two different scales. This implies that the nodal structure of the lowest quasiparticle band $E_3(\mathbf{k})$ does not coincide with the nodal structure of the order parameter matrix elements $\Delta_{\alpha\alpha}(\mathbf{k})$. The solid blue curve describes $\Delta_{\Uparrow\Uparrow}(\mathbf{k})$, which has an f-wave character (three nodes); the dashed red curve describes $\Delta_{00}(\mathbf{k})$, which has a p-wave character (one node); the dash-dotted green curve describes $\Delta_{\Downarrow\Downarrow}(\mathbf{k})$, which also has a p-wave character (one node).

In Fig. 7(b) we show the momentum dependence of the off-diagonal components $\Delta_{\alpha\beta}(\mathbf{k})$ of the order parameter tensor, with $\alpha \neq \beta$, in two cases. From these plots it is also evident that the nodal structure of the order parameter tensor components $\Delta_{\alpha\beta}(\mathbf{k})$ is exactly the same for the $R3$ and $R1$ phases. Again, the only difference between the two cases is the overall magnitude of the amplitude $|\Delta|$. As in the case of diagonal components, this implies that the nodal structure of the lowest quasiparticle band $E_3(\mathbf{k})$ does not coincide with the nodal structure of the off-diagonal matrix elements $\Delta_{\alpha\beta}(\mathbf{k})$. The solid brown curve describes $\Delta_{\Uparrow 0}(\mathbf{k})$, which has an f-wave character (two nodes and a discontinuous sign change); the dashed magenta curve describes $\Delta_{\Downarrow 0}(\mathbf{k})$, which has an f-wave character (two nodes and a discontinuous sign change); the dash-dotted orange curve describes $\Delta_{\Uparrow\Downarrow}(\mathbf{k})$, which has a p-wave character (one node).

A very important property that emerges from Figs. 7(a) and 7(b) is that the order parameter tensor $\Delta_{\alpha\beta}(\mathbf{k})$ for color superfluids (with three colors) is always an odd function of momentum $\mathbf{k}$ when the one-dimensional color-orbit coupling $h_z(\mathbf{k}) = 2k_T k_x/2m$ is present with zero color shift (detuning $\delta = 0$), meaning that the condition $\Delta_{\alpha\beta}(\mathbf{k}) = -\Delta_{\alpha\beta}(-\mathbf{k})$ is satisfied. The odd-parity condition combined with the Fermi statistics property $\Delta_{\alpha\beta}(\mathbf{k}) = -\Delta_{\beta\alpha}(-\mathbf{k})$ leads to a symmetric order parameter tensor $\Delta_{\alpha\beta}(\mathbf{k}) = \Delta_{\beta\alpha}(\mathbf{k})$ under mixed-color exchange $\alpha \leftrightarrow \beta$, when $k_T \neq 0$. Furthermore, the order parameter tensor is odd under reflection along the k_x direction, but even under reflections along the k_y and k_z directions.

As can be seen in Fig. 4(c), the nodal structure of quasiparticle excitations in the $R3$ phase is similar to that of the excitation spectrum of a fully spin-polarized triplet f-wave superfluid of spin-1/2 fermions with energy band $\xi_{\mathbf{k}} = \mathbf{k}^2/2m - \mu$ and order parameter amplitude $|\Delta_{\mathbf{k}}| = |a_f k_x^3 - a_p k_x|$, with a_f and a_p being positive. In this case, the quasiparticle excitation spectrum is simply $E(\mathbf{k}) = \sqrt{\xi_{\mathbf{k}}^2 + |\Delta_{\mathbf{k}}|^2}$ and the nodes $E_{\mathbf{k}}$ occur at the intersection of the surfaces $\xi_{\mathbf{k}} = 0$ and $|\Delta_{\mathbf{k}}| = 0$. Since the zeros of the order parameter are located at $k_x = 0$ and $k_x = \pm\sqrt{a_p/a_f}$, and the zeros of $\xi_{\mathbf{k}}$ are located at $(k_y^2 + k_z^2)/2m = \mu - k_x^2/2m$, the loci of zero quasiparticle energy have a three-ring structure. Additionally, the nodal structure of quasiparticle excitations in the superfluid state $R1$, shown in Fig. 4(d), is similar to that of a triplet p-wave superfluid of fully spin-polarized spin-1/2 fermions with order parameter amplitude $|\Delta_{\mathbf{k}}| = |a_p k_x|$. In this case, the nodes in $E(\mathbf{k})$ occur at the intersection of the surfaces $k_x = 0$ and $(k_y^2 + k_z^2)/2m = \mu - k_x^2/2m$, thus leading to a single-ring nodal structure for the loci of zero quasiparticle energy. It is important to emphasize, though, that in the color problem the location of zeros of the quasiparticle band $E_3(\mathbf{k})$ does not coincide with the simultaneous zeros of the order parameter tensor components $\Delta_{\alpha\beta}(\mathbf{k}) = 0$ and band dispersions $\xi_\alpha(\mathbf{k}) - \mu$.

It is also important to compare the momentum dependence of the order parameter tensor $\Delta_{\alpha\beta}(\mathbf{k})$ for the color problem with color-orbit and color-flip fields and the corresponding spin-1/2 problem with spin-orbit and Zeeman fields [46]. As shown in Figs. 7(a) and 7(b), the momentum dependence of $\Delta_{\alpha\beta}(\mathbf{k})$ shows higher angular momentum pairing in the color indices. It does so in a similar but more complicated fashion in comparison to the spin-1/2 case [46], where the 2×2 order parameter tensor $\Delta_{\alpha\beta}(\mathbf{k})$ in the generalized helicity basis $\{\Uparrow, \Downarrow\}$ acquires also a triplet component with dominant p-wave character. A particularly notable difference between the color case and the spin-1/2 case is that the order parameter tensor $\Delta_{\alpha\beta}(\mathbf{k})$ is a symmetric tensor when both color-orbit and color-flip fields are nonzero, that is, $\Delta_{\alpha\beta}(\mathbf{k}) = \Delta_{\beta\alpha}(\mathbf{k})$, while in the spin-1/2 the corresponding order parameter tensor $\Delta_{\alpha\beta}(\mathbf{k})$ is neither antisymmetric nor symmetric, that is, the off-diagonal elements $\Delta_{\Uparrow\Downarrow}(\mathbf{k})$ and $\Delta_{\Downarrow\Uparrow}(\mathbf{k})$ are neither equal nor opposite in sign. Therefore, the order parameter tensor has symmetric components $\Delta_{\Uparrow\Uparrow}(\mathbf{k})$, $[\Delta_{\Uparrow\Downarrow}(\mathbf{k}) + \Delta_{\Downarrow\Uparrow}(\mathbf{k})]/2$, and $\Delta_{\Downarrow\Downarrow}(\mathbf{k})$, corresponding to the triplet sector, and an antisymmetric component $[\Delta_{\Uparrow\Downarrow}(\mathbf{k}) - \Delta_{\Downarrow\Uparrow}(\mathbf{k})]/2$, corresponding to the singlet sector.

In the color problem discussed here, the tensor $\Delta_{\alpha\beta}(\mathbf{k})$ is only antisymmetric when the color-orbit field $h_z(\mathbf{k}) = 2k_T k_x/2m$ is zero, that is, the color-dependent momentum transfer $k_T = 0$. This jump from an antisymmetric tensor for zero color-orbit fields to a symmetric tensor for nonzero color-orbit fields arises due to the absence of color-gauge symmetry associated with the three-color states even when the color-flip field is zero. This singular perturbation caused by the color-orbit field $h_z(\mathbf{k})$ introduces only odd-parity momentum dependences in the mixed-color representation of the order parameter tensor, provided the color-shift field $\delta = 0$, as it is the case throughout this paper.

To highlight further the structure of the order parameter tensor in the color problem with color-flip and color-orbit fields, we discuss next its structure in the total pseudospin basis, where singlet, triplet, and quintet sectors emerge in a similar fashion to the singlet and triplet sectors that arise for the order parameter tensor of spin-1/2 Fermi superfluids with spin-orbit coupling and Zeeman fields.

B. Order parameter in the total pseudospin basis

In order to understand further the order parameter structure in the color problem, we also analyze it in the total pseudospin basis $|S,m_s\rangle$ built from the mixed-color states $\{|\Uparrow\rangle,|0\rangle,|\Downarrow\rangle\}\otimes\{|\Uparrow\rangle,|0\rangle,|\Downarrow\rangle\}$. The order parameter tensor in the total pseudospin basis $\widetilde{\Delta}_{Sm_s}(\mathbf{k})$ can be separated into singlet, triplet, and quintet sectors and can be written as $\widetilde{\Delta}_{Sm_s}(\mathbf{k})=M^{Sm_s}_{\alpha\beta}\Delta_{\alpha\beta(\mathbf{k})}$, where $M^{Sm_s}_{\alpha\beta}$ is a tensor whose elements represent generalized Clebsch-Gordon coefficients. The singlet sector is described by fermion pairs in the state $|Sm_s\rangle=|00\rangle$ with order parameter elements

$$\widetilde{\Delta}_{00}(\mathbf{k})=\frac{1}{\sqrt{3}}\Delta_{\Uparrow\Downarrow}(\mathbf{k})-\frac{1}{\sqrt{3}}\Delta_{00}(\mathbf{k})+\frac{1}{\sqrt{3}}\Delta_{\Downarrow\Uparrow}(\mathbf{k}),$$

while the triplet sector is characterized by fermions pairs in the states $\{|Sm_s\rangle\}=\{|11\rangle,|10\rangle,|1\bar{1}\rangle\}$, with order parameter elements

$$\widetilde{\Delta}_{11}(\mathbf{k})=\frac{1}{\sqrt{2}}\Delta_{\Uparrow 0}(\mathbf{k})-\frac{1}{\sqrt{2}}\Delta_{0\Uparrow}(\mathbf{k}),$$
$$\widetilde{\Delta}_{10}(\mathbf{k})=\frac{1}{\sqrt{2}}\Delta_{\Uparrow\Downarrow}(\mathbf{k})-\frac{1}{\sqrt{2}}\Delta_{\Downarrow\Uparrow}(\mathbf{k}),$$
$$\widetilde{\Delta}_{1\bar{1}}(\mathbf{k})=\frac{1}{\sqrt{2}}\Delta_{0\Downarrow}(\mathbf{k})-\frac{1}{\sqrt{2}}\Delta_{\Downarrow 0}(\mathbf{k}),$$

where we used the notation $\bar{1}=-1$. Finally, the quintet sector is described by fermion pairs in states $\{|Sm_s\rangle\}=\{|22\rangle,|21\rangle,|20\rangle,|2\bar{1}\rangle,|2\bar{2}\rangle\}$, with order parameter elements

$$\widetilde{\Delta}_{22}(\mathbf{k})=\Delta_{\Uparrow\Uparrow}(\mathbf{k}),$$
$$\widetilde{\Delta}_{21}(\mathbf{k})=\frac{1}{\sqrt{2}}\Delta_{\Uparrow 0}(\mathbf{k})+\frac{1}{\sqrt{2}}\Delta_{0\Uparrow}(\mathbf{k}),$$
$$\widetilde{\Delta}_{20}(\mathbf{k})=\frac{1}{\sqrt{6}}\Delta_{\Uparrow\Downarrow}(\mathbf{k})+\sqrt{\frac{2}{3}}\Delta_{00}(\mathbf{k})+\frac{1}{\sqrt{6}}\Delta_{\Downarrow\Uparrow}(\mathbf{k}),$$
$$\widetilde{\Delta}_{2\bar{1}}(\mathbf{k})=\frac{1}{\sqrt{2}}\Delta_{0\Downarrow}(\mathbf{k})+\frac{1}{\sqrt{2}}\Delta_{\Downarrow 0}(\mathbf{k}),$$
$$\widetilde{\Delta}_{2\bar{2}}(\mathbf{k})=\Delta_{\Downarrow\Downarrow}(\mathbf{k}),$$

where we used the notation $\bar{m}_s=-m_s$.

From the linear combinations given above, we can see that the order parameter components in the singlet and quintet sectors are symmetric with respect to mixed-color exchange, while those in the triplet sector are antisymmetric with respect to mixed-color exchange. However, for nonzero color-orbit coupling and color-flip field, but a zero color shift ($\delta=0$), the tensor $\Delta_{\alpha\beta}(\mathbf{k})$ is symmetric in mixed-color indices and thus the only nonvanishing components of $\widetilde{\Delta}_{Sm_s}(\mathbf{k})$ occur in the singlet or quintet sectors, while all the components in the triplet sector vanish identically. In Figs. 7(c) and 7(d) we show the nonvanishing components of $\widetilde{\Delta}_{Sm_s}(\mathbf{k})$.

In Figs. 7(c) and 7(d) the momentum dependences of the order parameter tensor $\widetilde{\Delta}_{Sm_s}(\mathbf{k})$ are the same for the $R3$ and $R1$ superfluid phases for fixed Ω/E_F and varying $1/k_Fa_s$, but the overall magnitude is different. Again, this shows that the nodes in the quasiparticle band $E_3(\mathbf{k})$ are not trivially related to the nodes of the order parameter tensor $\widetilde{\Delta}_{Sm_s}(\mathbf{k})$. In Fig. 7(c) the solid yellow curve corresponds to $\widetilde{\Delta}_{22}(\mathbf{k})$, the dashed cyan curve indicates $\widetilde{\Delta}_{21}(\mathbf{k})$, and the dash-dotted purple curve describes $\widetilde{\Delta}_{20}(\mathbf{k})$. Notice that $\widetilde{\Delta}_{22}(\mathbf{k})$ has an f-wave character (three nodes), $\widetilde{\Delta}_{21}(\mathbf{k})$ has also an f-wave character (two nodes and one discontinuous sign change), and $\widetilde{\Delta}_{20}(\mathbf{k})$ has a p-wave character (one node). In Fig. 7(d) the solid light blue line indicates $\widetilde{\Delta}_{2\bar{1}}(\mathbf{k})$, the dashed red line shows $\widetilde{\Delta}_{2\bar{2}}(\mathbf{k})$, and the dash-dotted black line describes $\widetilde{\Delta}_{00}(\mathbf{k})$. Notice that $\widetilde{\Delta}_{2\bar{1}}(\mathbf{k})$ has an f-wave character (two nodes and a discontinuous sign change), $\widetilde{\Delta}_{2\bar{2}}(\mathbf{k})$ has a p-wave character (one node), and $\widetilde{\Delta}_{00}(\mathbf{k})$ also has a p-wave character (one node). Finally, since the mixed-color order parameter tensor $\Delta_{\alpha\beta}(\mathbf{k})$ is symmetric in $\alpha\leftrightarrow\beta$, the triplet sector tensor components $\widetilde{\Delta}_{1,1}(\mathbf{k})$, $\widetilde{\Delta}_{1,0}(\mathbf{k})$, and $\widetilde{\Delta}_{1,\bar{1}}(\mathbf{k})$ all vanish identically and thus these components are not shown in Fig. 7.

In order to understand better color pairing phenomena and color superfluid phases, we discuss next spectroscopic properties, such as the quasiparticle excitation spectrum obtained via pairing in the mixed-color basis, as well as momentum distributions and the density of states of fermions in their original colors $\{R,G,B\}$.

V. SPECTROSCOPIC PROPERTIES

In this section we discuss several spectroscopic properties of color superfluids in the presence of color-orbit coupling and color-flip fields. These spectroscopic properties can help characterize the different topological phases that emerge for fixed color-orbit coupling but changing color-flip fields Ω/E_F and interactions $1/k_Fa_s$. We begin our discussion by analyzing the quasiparticle and quasihole excitation spectrum.

A. Quasiparticle energy spectrum

To investigate in detail the quasiparticle and quasihole excitation spectrum, it is easier to start from the Hamiltonian written in the mixed-color basis $\{\Uparrow,0,\Downarrow\}$ as described in Eq. (19). In this case, the matrix $\mathbf{H}_M(\mathbf{k})$ has only diagonal elements $\{\xi_{\Uparrow}(\mathbf{k}),\xi_0(\mathbf{k}),\xi_{\Downarrow}(\mathbf{k})\}$ corresponding to mixed-color particle energies. Furthermore, the matrix $-\mathbf{H}^*_M(-\mathbf{k})$ also has only diagonal elements $\{-\xi_{\Uparrow}(-\mathbf{k}),-\xi_0(-\mathbf{k}),-\xi_{\Downarrow}(-\mathbf{k})\}$ corresponding to mixed-color hole energies. The matrices Δ_M and $\Delta^{\dagger}_M$ are characterized by the elements $[\Delta_M]_{\alpha\beta}=\Delta_{\alpha\beta}(\mathbf{k})$ and $[\Delta^{\dagger}_M]_{\alpha\beta}=\Delta^*_{\beta\alpha}(\mathbf{k})$, which couple mixed-color bands with indices $\{\alpha,\beta\}=\{\Uparrow,0,\Downarrow\}$ and thus tend to lift degeneracies between particle $\xi_{\alpha}(\mathbf{k})$ and hole $-\xi_{\beta}(-\mathbf{k})$ mixed-color bands.

The quasiparticle and quasihole excitation spectrum can be found analytically from the secular equation $\det[\omega\mathbf{1}-\widetilde{H}_0(\mathbf{k})]=0$. Notice that $P(\omega)=\det[\omega\mathbf{1}-\widetilde{H}_0(\mathbf{k})]=\prod_j[\omega-E_j(\mathbf{k})]$ is in general a polynomial of order 6 and admits six eigenvalues $E_j(\mathbf{k})$, three of them with positive energy corresponding to quasiparticles and three with negative energy corresponding to quasiholes. Since the eigenvalues of the Hamiltonian matrix are independent of the basis representation that is used, we recover the same eigenvalues as those from the direct diagonalization of the Hamiltonian matrix in the original color basis $\{c,c'\}=\{R,G,B\}$.

Recall that the Hamiltonian $\widetilde{H}_0(\mathbf{k})$ is particle-hole symmetric, implying that its eigenvalues $E_j(\mathbf{k})$ satisfy the quasiparticle-quasihole symmetry $E_j(\mathbf{k})=-E_{7-j}(-\mathbf{k})$, and in the case of zero color-shift field $\delta=0$, where parity is a good quantum number, the eigenvalues are parity even, satisfying

the relation $E_j(\mathbf{k}) = E_j(-\mathbf{k})$. In this case, the characteristic polynomial becomes $P(\omega) = a_0(\mathbf{k}) + a_2(\mathbf{k})\omega^2 + a_4(\mathbf{k})\omega^4 + \omega^6$. The nodal structure can be found by setting $\omega = 0$ and coincides with the results for the original Hamiltonian matrix, that is, $a_0(\mathbf{k}) = 0$ leads to the same nodal structure previously obtained. At this point it is illustrative to compare the present situation in color Fermi superfluids with that of spin-1/2 Fermi superfluids, where the nodal structure in the quasiparticle energies is directly related to the nodal structure of the 2×2 order parameter tensor $\Delta_{\alpha\beta}(\mathbf{k})$ or more precisely related to the nodal structure of $\Delta_{Sm_s}(\mathbf{k})$ in the singlet and triplet sectors [46]. The situation for color Fermi superfluids is very different, given that the coefficient $a_0(\mathbf{k})$ depends in a nontrivial way not only on the components of the $\Delta_{\alpha\beta}(\mathbf{k})$, but also on the eigenenergies $\xi_\alpha(\mathbf{k})$ of the mixed-color states $\{\Uparrow,0,\Downarrow\}$.

Given that the Hamiltonian matrix $\widetilde{H}_0(\mathbf{k})$ is Hermitian, its eigenvalues are guaranteed to be real, so the discriminant $\mathcal{D}$ of the cubic equation obtained with the substitution $z = \omega^2$ is always nonpositive, that is, $\mathcal{D} \leqslant 0$. The cubic equation obtained can be written as $P_3(z) = c + bz + az^2 + z^3$, where $c = a_0(\mathbf{k})$, $b = a_2(\mathbf{k})$, and $a = a_4(\mathbf{k})$, and can be solved exactly using the Cardano method [54]. The discriminant can be obtained from the auxiliary functions $Q = (3b - a^2)/9$ and $R = (9ab - 27c - 2a^3)/54$ as $\mathcal{D} = Q^3 + R^2$. If $\mathcal{D} \leqslant 0$, it is clear that $Q^3 = \mathcal{D} - R^2$ is also negative and thus both $-Q^3$ and $-Q$ are positive. If we let $\cos(\theta) = R/\sqrt{-Q^3}$, then the three real roots of $P_3(z)$ are $z_1 = 2\sqrt{-Q}\cos(\theta/3) - a/3$, $z_2 = 2\sqrt{-Q}\cos[(\theta + 2\pi)/3] - a/3$, and $z_3 = 2\sqrt{-Q}\cos[(\theta + 4\pi)/3)] - a/3$. The three roots of the cubic polynomial $P_3(z)$ correspond to the squares of the excitations energies $E_j^2(\mathbf{k})$ and thus lead to the six solutions $E_j(\mathbf{k})$ that we are seeking. The positive-energy solutions $E_1(\mathbf{k})$, $E_2(\mathbf{k})$, and $E_3(\mathbf{k})$ correspond to quasiparticle excitations and the negative-energy solutions $E_4(\mathbf{k})$, $E_5(\mathbf{k})$, and $E_6(\mathbf{k})$ correspond to quasihole excitations. The analytic solutions for $E_j(\mathbf{k})$ agree with the direct numerical diagonalization of either $\mathbf{H}_0(\mathbf{k})$ in the color basis $\{R,G,B\}$ defined in Eq. (13) or $\widetilde{\mathbf{H}}_0(\mathbf{k})$ in the mixed-color basis $\{\Uparrow,0,\Downarrow\}$ defined in Eq. (19). However, the reader must agree that these analytic solutions are not particularly illuminating.

In order to understand the excitation spectrum obtained on physical grounds, it is more convenient to work in the mixed-color basis $\{\Uparrow,0,\Downarrow\}$. The excitation spectra shown in Fig. 8 can be generically understood as resulting from the coupling of mixed-color particle states with energies $\mathcal{E}_\alpha(\mathbf{k})$ and mixed-color hole states with energies $-\mathcal{E}_\beta(-\mathbf{k})$ via the order parameter $\Delta_{\alpha\beta}(\mathbf{k})$. Thus, wherever the energies $\mathcal{E}_\alpha(\mathbf{k})$ and $-\mathcal{E}_\beta(-\mathbf{k})$ cross in momentum space, the order parameter matrix elements $\Delta_{\alpha\beta}(\mathbf{k})$ can lift the degeneracies between the bands labeled by α and β at the crossing loci (points, lines, and surfaces) and impound additional momentum dependence.

In Fig. 8 we show representative quasiparticle and quasihole energies $E_j(\mathbf{k})$ versus momentum $\mathbf{k}$ in superfluid phases $R3$ and $R1$ for fixed parameters $\Omega/E_F = 0.29$, $k_T = 0.35k_F$, $T/E_F = 0.01$, and $b_z = k_T^2/2m$. The spectrum is sorted out such that $E_1(\mathbf{k})$ is the highest energy and $E_6(\mathbf{k})$ is the lowest energy for fixed $\mathbf{k}$. The solid blue curves correspond to $E_1(\mathbf{k})$, the dashed red plots describe $E_2(\mathbf{k})$, the dotted green lines show $E_3(\mathbf{k})$, the dash-dotted cyan curves correspond to $E_4(\mathbf{k})$, the dash–double-dotted brown plots describe $E_5(\mathbf{k})$, and the double-dash–dotted magenta lines show $E_6(\mathbf{k})$. The excitation spectrum $E_j(\mathbf{k})$ has cylindrical symmetry around the k_x axis and thus its momentum dependence (k_x,k_y,k_z) is characterized only by the coordinates $(k_x,k_\perp)$, where $k_\perp = \sqrt{k_y^2 + k_z^2}$ is the magnitude of momentum in the (k_y,k_z) plane.

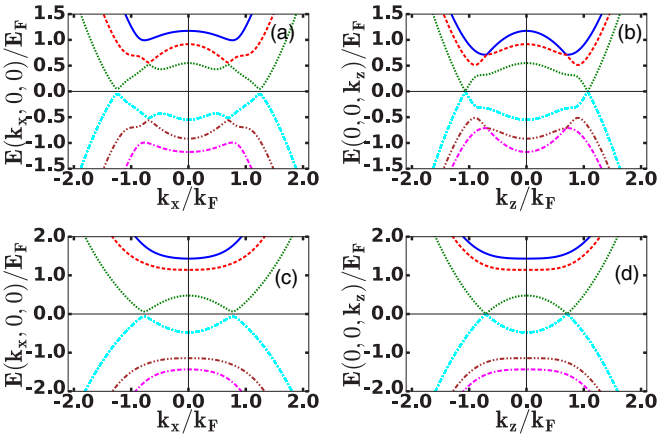

FIG. 8. Quasiparticle and quasihole excitation spectra $E_j(\mathbf{k})$ in superfluid phases $R3$ and $R1$ for fixed parameters $\Omega/E_F = 0.29$, $k_T = 0.35k_F$, $T/E_F = 0.01$, and $b_z = k_T^2/2m$. The style and color code for energies $E_j(\mathbf{k})$ is $E_1(\mathbf{k})$, solid blue; $E_2(\mathbf{k})$, dashed red; $E_3(\mathbf{k})$, dotted green; $E_4(\mathbf{k})$, dash-dotted cyan; $E_5(\mathbf{k})$, dash–double-dotted brown; and $E_6(\mathbf{k})$, double-dash–dotted magenta. We show $E_j(\mathbf{k})$ versus (a) $(k_x,0,0)$ and (b) $(0,0,k_z)$ for the $R3$ phase with the parameters $1/k_Fa_s = -0.069$, $\mu/E_F = 0.81$, and $|\Delta|/E_F = 0.31$ and $E_j(\mathbf{k})$ versus (c) $(k_x,0,0)$ and (d) $(k_x = 0,0,k_z)$ for the $R1$ phase with the parameters $1/k_Fa_s = 0.62$, $\mu/E_F = 0.19$, and $|\Delta|/E_F = 0.73$.

In Figs. 8(a) and 8(b) we show $E_j(\mathbf{k})$ versus $(k_x,0,0)$ and $(0,0,k_z)$, respectively, for the $R3$ phase with the parameter $1/k_Fa_s = -0.069$ ($\mu/E_F = 0.81$ and $|\Delta|/E_F = 0.31$). Notice that only one ring of nodes is illustrated in Fig. 8(b) where $k_x = 0$, since the nodal points in k_z correspond to a ring of nodes in the (k_y,k_z) plane due to cylindrical symmetry. The other two rings of nodes for the $R3$ phase occur at characteristic values $k_x = \pm k_x^* \neq 0$ and $k_\perp = k_\perp^* \neq 0$ as found in Fig. 4(c). The additional rings of the $R3$ phase are not seen in the spectrum shown in Fig. 8, because in Fig. 8(a) the magnitude of the momentum in the (k_y,k_z) plane is $k_\perp = 0$ and in Fig. 8(b) the momentum along the k_x direction is $k_x = 0$.

In Figs. 8(c) and 8(d) we show $E_j(\mathbf{k})$ versus $(k_x,0,0)$ and $(0,0,k_z)$, respectively, for the $R1$ phase with the parameter $1/k_Fa_s = 0.62$ ($\mu/E_F = 0.19$ and $|\Delta|/E_F = 0.73$). The $R1$ phase has only one ring of nodes [see Fig. 4(d)] and this ring is illustrated in the spectrum shown in Fig. 8(d), where $k_x = 0$ and the nodal points in k_z correspond to a ring of nodes in the (k_y,k_z) plane.

We would like to point out that photoemission spectroscopy has been already used to probe directly the elementary excitations and energy dispersion in a strongly interacting Fermi gas of ^{40}K atoms with two internal states throughout the evolution from the BCS to the BEC limits [61], but without spin-orbit coupling or Zeeman fields. The use of the same technique for the color problem with ^{6}Li, ^{40}K, or ^{173}Yb should reveal the rich nodal structure of the excitation spectrum when color-orbit and color-flip fields are present and thus provide direct evidence of

the various topological superfluid phases shown in the phase diagram of Fig. 3(a).

In addition to measuring the quasiparticle dispersions, there are other auxiliary experiments than can help characterize the quantum phases found in the color problem. Therefore, we analyze next the momentum distribution $n_c(\mathbf{k})$ for color states $c = \{R,G,B\}$ as color-flip fields and interactions are changed for fixed color-orbit coupling.

B. Momentum distribution

The measurement of momentum distributions is an easy experiment to do in systems of cold atoms and it is routinely realized in atomic fermions and bosons. More recently these types of measurements have also been performed in ultracold fermions such as ^{40}K with two internal states and spin-orbit coupling [38], as well as ^{173}Yb with three or more internal states and spin-orbit coupling [33].

Therefore, in this section we describe how the momentum distribution $n_c(\mathbf{k})$ for different color states $c = \{R,G,B\}$ can be obtained directly from the resolvent operator

$$\hat{\mathbf{G}}(z) = [z\hat{\mathbf{I}} - \hat{\mathbf{H}}]^{-1}, \tag{21}$$

where z is a complex energy, $\hat{\mathbf{I}}$ is the identity operator, and $\hat{\mathbf{H}}$ is the full Hamiltonian of the system. In the present case, the resolvent operator can be written in energy and momentum space as the 6×6 matrix

$$\mathbf{G}_{\nu\nu'}(z,\mathbf{k}) = [z\mathbf{I} - \mathbf{H}_0(\mathbf{k})]^{-1}_{\nu\nu'}, \tag{22}$$

where $\mathbf{H}_0(\mathbf{k})$ is the Hamiltonian matrix defined in Eq. (13) describing the color superfluid phases at low temperatures and $\{\nu,\nu'\}$ are Nambu color indices representing the states created by the six-dimensional colored Nambu spinor $\mathbf{f}^\dagger_N(\mathbf{k}) = [f^\dagger_R(\mathbf{k}), f^\dagger_G(\mathbf{k}), f^\dagger_B(\mathbf{k}), f_R(-\mathbf{k}), f_G(-\mathbf{k}), f_B(-\mathbf{k})]$, which was defined in Sec. III A.

Writing the eigenstates of the Hamiltonian matrix $\mathbf{H}_0(\mathbf{k})$ as $|j,\mathbf{k}\rangle = \mathbf{M}_{j\nu}(\mathbf{k})|\nu,\mathbf{k}\rangle$ in terms of the Nambu color states $|\nu,\mathbf{k}\rangle$ and using the corresponding eigenvalues $E_j(\mathbf{k})$ leads to the Green's function matrix

$$\mathbf{G}_{\nu\nu'}(z,\mathbf{k}) = \sum_j \frac{M_{j\nu}(\mathbf{k})M^*_{\nu' j}(\mathbf{k})}{z - E_j(\mathbf{k})}. \tag{23}$$

The momentum distribution for color state c can be written as $n_c(\mathbf{k}) = -T\sum_{i\omega_n} \mathbf{G}_{cc}(i\omega_n,\mathbf{k})$, where $\mathbf{G}_{cc}(i\omega_n,\mathbf{k})$ are the first three diagonal elements of $\mathbf{G}_{\nu\nu'}(z = i\omega_n,\mathbf{k})$, T is the temperature, and $\omega_n = (2n+1)\pi/T$ are the fermionic Matsubara frequencies. Performing the Matsubara sums leads to the momentum distribution

$$n_c(\mathbf{k}) = \sum_j |\mathbf{M}_{jc}(\mathbf{k})|^2 F[E_j(\mathbf{k})], \tag{24}$$

where the matrix element $\mathbf{M}_{jc}(\mathbf{k})$ represents the probability amplitude of finding the color state $|c,\mathbf{k}\rangle$ as part of the eigenstate $|j,\mathbf{k}\rangle$ and $|\mathbf{M}_{jc}(\mathbf{k})|^2 = \mathbf{M}_{jc}(\mathbf{k})\mathbf{M}^*_{cj}(\mathbf{k})$. Here $F[E_j(\mathbf{k})]$ is the Fermi function associated with eigenenergy $E_j(\mathbf{k})$ and the summation over j includes both quasiparticle and quasihole states, that is, j runs from 1 to 6.

In Figs. 9(a)–9(d) we show momentum distributions $n_c(\mathbf{k})$ for $\Omega = 0.29E_F$, $k_T = 0.35k_F$, $b_z = k_T^2/2m$, and $T = 0.01E_F$ that describe the normal phase $N3$ in Fig. 9(a) with the scattering parameter $1/k_Fa_s = -1.8$ ($\mu/E_F = 0.97$ and $|\Delta|/E_F = 0.0$); the three-ring superfluid phase $R3$ in Fig. 9(b) with the scattering parameter $1/k_Fa_s = -0.069$ ($\mu/E_F = 0.81$ and $\Delta/E_F = 0.31$), the one-ring superfluid phase $R1$ in Fig. 9(c) with the scattering parameter $1/k_Fa_s = 0.62$ ($\mu/E_F = 0.19$ and $|\Delta|/E_F = 0.73$), and the fully gapped superfluid phase FG in Fig. 9(d) with the scattering parameter $1/k_Fa_s = 1.8$ ($\mu/E_F = -2.88$ and $|\Delta|/E_F = 1.25$).

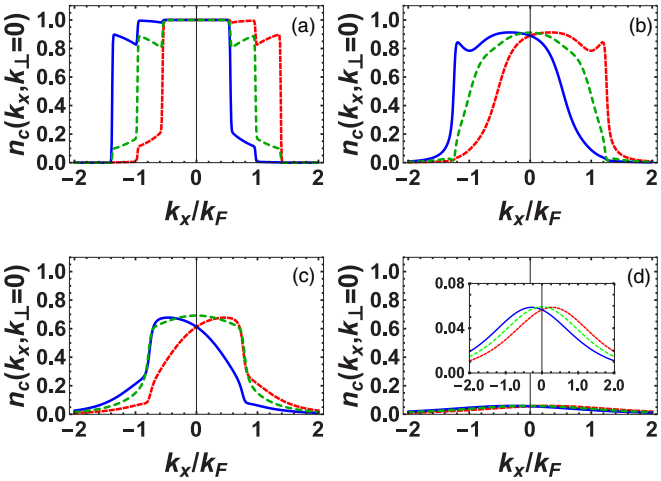

FIG. 9. Momentum distributions $n_c(\mathbf{k})$ for $\Omega = 0.29E_F$, $k_T = 0.35k_F$, $b_z = k_T^2/2m$, and $T = 0.01E_F$ along direction $(k_x,0,0)$ for different color indices $c = \{R,G,B\}$. The solid blue lines correspond to blue states, the long-dashed green lines to green states, and the short-dashed red lines to red states. Plots are shown for (a) the normal phase $N3$ with the scattering parameter $1/k_Fa_s = -1.8$ ($\mu/E_F = 0.97$ and $|\Delta|/E_F = 0.0$), (b) the three-rings superfluid phase $R3$ with the scattering parameter $1/k_Fa_s = -0.069$ ($\mu/E_F = 0.81$ and $|\Delta|/E_F = 0.31$), (c) the one-ring superfluid phase $R1$ with the scattering parameter $1/k_Fa_s = 0.62$ ($\mu/E_F = 0.19$ and $|\Delta|/E_F = 0.73$), and (d) the fully gapped superfluid phase FG with the scattering parameter $1/k_Fa_s = 1.8$ ($\mu/E_F = -2.88$ and $|\Delta|/E_F = 1.25$).

A general key feature of the momentum distributions shown in Fig. 9 is that the distributions of red fermions are shifted to the right (towards positive k_x) and that of the blue fermions are shifted to the left (towards negative k_x), while the distribution of green fermions remain centered at zero momentum. A second general feature revealed by Fig. 9 is that the momentum distributions get smeared and broadened along k_x by the emergence of the order parameter of the superfluid state and by increasing scattering parameter. This leads to an overall reduction of the maximum values of the momentum distributions, making the fermionic system less degenerate, similarly to the case of two internal states, that is, the spin-1/2 case. Another important observation about Fig. 9 is that the momentum distributions $n_R(\mathbf{k})$ of the red (R) states and $n_B(\mathbf{k})$ of the blue (B) states satisfy the relation $n_R(\mathbf{k}) = n_B(-\mathbf{k})$, because the quasiparticle and quasihole energies are even functions of momentum $E_j(-\mathbf{k}) = E_j(\mathbf{k})$ and the matrix elements $M_{jR}(\mathbf{k}) = M_{jB}(-\mathbf{k})$. The latter symmetry relation follows from the fact that the R and B states experience momentum shifts k_T in opposite directions.

In Fig. 10 we show the momentum distributions $n_c(\mathbf{k})$ for zero color-orbit coupling $k_T = 0$, zero quadratic color

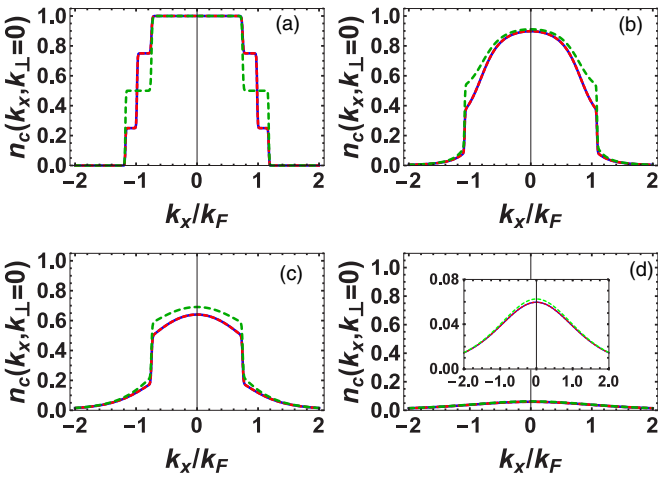

FIG. 10. Momentum distributions $n_c(\mathbf{k})$ for $k_T = 0$ and $b_z = k_T^2/2m = 0$ at $T = 0.01E_F$ along direction $(k_x,0,0)$ for different color indices $c = \{R,G,B\}$. The solid blue lines correspond to the blue states, the long-dashed green lines to the green states, and the short-dashed red lines to the red states. Plots are shown for (a) the normal phase $N3$ with the scattering parameter $1/k_Fa_s = -1.8$ ($\mu/E_F = 0.97$ and $|\Delta|/E_F = 0.0$), (b) the superfluid phase $S1$ with the scattering parameter $1/k_Fa_s = -0.069$ ($\mu/E_F = 0.78$ and $|\Delta|/E_F = 0.33$), (c) the superfluid phase $S1$ with the scattering parameter $1/k_Fa_s = 0.62$ ($\mu/E_F = 0.17$ and $|\Delta|/E_F = 0.73$), and (d) the fully gapped superfluid phase FG with the scattering parameter $1/k_Fa_s = 1.8$ ($\mu/E_F = -2.88$ and $|\Delta|/E_F = 1.25$).

shift $b_z = k_T^2/2m = 0$, and finite color-flip field $\Omega/E_F = 0.29$ at $T = 0.01E_F$. The distributions are shown along direction $(k_x,0,0)$ for different color indices $c = \{R,G,B\}$ and can be contrasted with those of Fig. 9, where the color-orbit coupling is $k_T = 0.35k_F$. To facilitate comparison between Figs. 9 and 10, we use the same scattering parameters for corresponding panels. In Fig. 10(a) we show plots for the normal phase $N3$ with the scattering parameter $1/k_Fa_s = -1.8$ ($\mu/E_F = 0.97$ and $|\Delta|/E_F = 0.0$). In Fig. 10(b) we show plots for the superfluid phase $S1$ with scattering parameter $1/k_Fa_s = -0.069$ ($\mu/E_F = 0.78$ and $|\Delta|/E_F = 0.33$). In Fig. 10(c) we show plots for the superfluid phase $S1$ with the scattering parameter $1/k_Fa_s = 0.62$ ($\mu/E_F = 0.17$ and $|\Delta|/E_F = 0.73$). In Fig. 10(d) we show plots for the fully gapped superfluid phase FG with the scattering parameter $1/k_Fa_s = 1.8$ ($\mu/E_F = -2.88$ and $|\Delta|/E_F = 1.25$). Notice that the interaction parameters and color-flip fields are exactly the same as those of the corresponding panels in Fig. 9 and were chosen as such in order to illustrate the effect of the color-orbit coupling k_T.

Momentum distributions are relatively easy to measure experimentally in the case of two internal states and there should be no additional difficulties in measuring them for the case of color states. However, it is important to emphasize that only measurements of the quasiparticle and quasihole excitation spectrum can identify fully each of the topological superfluid phases and their nodal structure, as discussed in Sec. V A.

A general feature of the momentum distributions shown in Fig. 10 is that the distributions of red and blue fermions are not shifted with respect to that of the green fermions, because there is no color-orbit coupling ($k_T = 0$) and thus no color-dependent momentum transfer. A second general feature revealed by the panels of Fig. 10 is that the momentum distributions get smeared and broadened along k_x by the emergence of the order parameter of the superfluid and by the increasing scattering parameter. This leads to an overall reduction of the maximum values of the momentum distributions, making the fermionic system less degenerate, similarly to the case of Fig. 9, where the color-orbit coupling is nonzero ($k_T \neq 0$). Another important observation about Fig. 10 is that the momentum distributions $n_R(\mathbf{k})$ of the red (R) states and $n_B(\mathbf{k})$ of the blue (B) states are identical, that is, $n_R(\mathbf{k}) = n_B(\mathbf{k})$, because the matrix elements $M_{jR}(\mathbf{k})$ and $M_{jB}(\mathbf{k})$ in Eq. (24) satisfy the relation $|M_{jR}(\mathbf{k})|^2 = |M_{jB}(\mathbf{k})|^2$. This implies that the R and B states can no longer be distinguished by measurements of their momentum distribution since they do not experience momentum shifts in opposite directions, that is, $k_T = 0$.

In order to sharpen our understanding of spectroscopic properties of color superfluids in the presence of color-orbit coupling and color-flip fields, we will discuss next the density of states for each color.

C. Color density of states

The density of states $\rho_c(\omega)$ for each color $c = \{R,G,B\}$ can be obtained from the Green's function defined in Eq. (23) as

$$\rho_c(\omega) = -\frac{1}{\pi}\sum_{\mathbf{k}} \lim_{\delta\to 0} \mathcal{I}[G_{cc}(z = \omega + i\delta,\mathbf{k})], \qquad (25)$$

where $\mathcal{I}$ denotes the imaginary part. Taking the limit of $\delta \to 0$ leads to the simplified expression

$$\rho_c(\omega) = \sum_{\mathbf{k},j} |\mathbf{M}_{jc}(\mathbf{k})|^2 \delta[\omega - E_j(\mathbf{k})], \qquad (26)$$

where the sum over $j = \{1,\ldots,6\}$ spans over all quasiparticle and quasihole states.

In Fig. 11 we show plots of frequency ω/E_F versus the density of the states $\rho_c(\omega/E_F)$ and the corresponding excitation spectrum $E_j(\mathbf{k})$ along the k_x direction, for the parameters $\Omega = 0.29E_F$, $k_T = 0.35k_F$, and $b_z = k_T^2/2m$ at temperature $T = 0.01E_F$. Figures 11(a) and 11(b) correspond to the normal phase $N3$ with the parameter $1/k_Fa_s = -1.8$ ($\mu/E_F = 0.97$ and $|\Delta|/E_F = 0$). Figures 11(c) and 11(d) correspond to the superfluid phase $R3$ with the parameter $1/k_Fa_s = -0.069$ ($\mu/E_F = 0.81$ and $|\Delta|/E_F = 0.31$). Figures 11(e) and 11(f) correspond to the superfluid phase $R1$ with the parameter $1/k_Fa_s = 0.62$ ($\mu/E_F = 0.19$ and $|\Delta|/E_F = 0.73$). Figures 11(g) and 11(h) correspond to the superfluid phase FG with the parameter $1/k_Fa_s = 1.1$ ($\mu/E_F = -0.73$ and $|\Delta|/E_F = 0.99$). A general feature of all the panels in Fig. 11 is that the density of states of the blue and red colors is identical, that is, $\rho_B(\omega/E_F) = \rho_R(\omega/E_F)$. This symmetry is ultimately connected to the shifts in the color dispersions $\varepsilon_R(\mathbf{k}) = \varepsilon(\mathbf{k} - \mathbf{k_T})$ to positive momenta and $\varepsilon_B(\mathbf{k}) = \varepsilon(\mathbf{k} + \mathbf{k_T})$ to negative momenta, which together with the evenness of $\varepsilon(\mathbf{k})$ leads to the relationship $\varepsilon_R(\mp\mathbf{k}) = \varepsilon_B(\pm\mathbf{k})$. This color-parity symmetry leads to identical density of states for the red and blue colored fermions, since it is no longer possible to distinguish between red and blue fermions after integration over momentum states. This last observation is an explicit

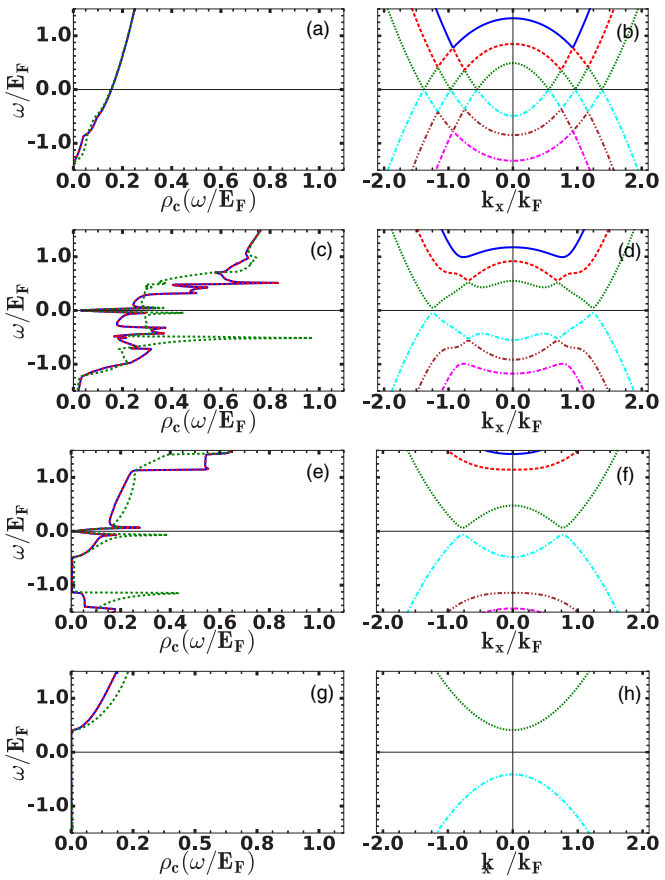

FIG. 11. Frequency ω/E_F versus color density of states $\rho_c(\omega/E_F)$ in the original $c = \{R,G,B\}$ basis and the corresponding excitation spectrum $E_j(\mathbf{k})$ along the k_x direction. The parameters used are $\Omega = 0.29E_F, k_T = 0.35k_F, b_z = k_T^2/2m$ at temperature $T = 0.01E_F$, and various interactions. In (a), (c), (e), and (g) the red dotted line represents the red fermions, the dashed green line represents the green fermions, and the blue solid line represents the blue fermions. In (b), (d), (f), and (h) the style and color code for energies $E_j(\mathbf{k})$ is $E_1(\mathbf{k})$, solid blue; $E_2(\mathbf{k})$, dashed red; $E_3(\mathbf{k})$, dotted green; $E_4(\mathbf{k})$, dash-dotted cyan; $E_5(\mathbf{k})$, dash–double-dotted brown; and $E_6(\mathbf{k})$, double-dash–dotted magenta. (a) and (b) Normal phase $N3$ with $1/k_Fa_s = -1.8$ ($\mu/E_F = 0.97$ and $|\Delta|/E_F = 0$). (c) and (d) Superfluid phase $R3$ with $1/k_Fa_s = -0.069$ ($\mu/E_F = 0.81$ and $|\Delta|/E_F = 0.31$). (e) and (f) Superfluid phase $R1$ with $1/k_Fa_s = 0.62$ ($\mu/E_F = 0.19$ and $|\Delta|/E_F = 0.73$). (g) and (h) Superfluid phase FG with $1/k_Fa_s = 1.1$ ($\mu/E_F = -0.73$ and $|\Delta|/E_F = 0.99$).

consequence of the symmetry relations for the matrix element $M_{j,R}(\pm\mathbf{k}) = M_{j,B}(\mp\mathbf{k})$ and for the quasiparticle and quasihole energies $E_j(\mathbf{k}) = E_j(-\mathbf{k})$, which follow from the fact that the red (R) and blue (B) states get momentum kicks k_T in opposite directions. Another overall feature of the plots is that cusps and peaks in the density of states $\rho_c(\omega/E_F)$ are associated with maxima, minima, and flat regions in the energy dispersions $E_j(\mathbf{k})$.

In Fig. 11(a) the color density of states $\rho_c(\omega/E_F)$ of the normal phase $N3$ with nonzero Ω/E_F and k_T/k_F has similar features to those of the normal state when Ω/E_F and k_T/k_F are zero and the red, green, and blue color states are degenerate. However, nonzero Ω/E_F and k_T/k_F mix the original R, G, and B states and lift degeneracies, making the density of states of the green fermions different from that of the red and blue fermions; the density of states of red and blue fermions, though, remains the same because of the color-parity symmetry $\varepsilon_R(\mp\mathbf{k}) = \varepsilon_B(\pm\mathbf{k})$. The corresponding quasiparticle-quasihole spectrum is shown in Fig. 11(b).

In Fig. 11(c) the color density of states for the $R3$ superfluid phase is illustrated. At low frequencies $|\omega|/E_F \ll |\Delta|/E_F$ the density of states grows linearly with frequency ω, that is, $\rho_c(\omega/E_F) = \gamma_c\omega/E_F$, because of the three nodal lines (rings) in the excitation spectrum. The coefficient γ_c depends on color. In the present case $\gamma_R = \gamma_B \neq \gamma_G$. Peaks in the color density of states appear at maxima and minima of the quasiparticle-quasihole excitation spectrum, as can be seen from the plots in Figs. 11(c) and 11(d).

In Fig. 11(e) the color density of states for the $R1$ superfluid phase is shown. Again, the color density of states is $\rho_c(\omega/E_F) = \gamma_c\omega/E_F$ for low frequencies, because there is a nodal line (ring) in the excitation energies $E_j(\mathbf{k})$. In the $R1$ phase, the coefficient γ_c is color dependent with $\gamma_R = \gamma_B \neq \gamma_G$ similarly to the $R3$ phase. Again, peaks in $\rho_c(\omega/E_F)$ appear at maxima and minima of the quasiparticle-quasihole excitation spectrum, as can be seen in Figs. 11(e) and 11(f).

In Fig. 11(g) the color density of states for the FG superfluid phase is shown. There is now a clear gap E_g in the color density of states $\rho_c(\omega/E_F)$, as can be seen in the excitation spectrum $E_j(\mathbf{k})$ shown in Fig. 11(h). Deep in this phase, where the scattering parameter $1/k_Fa_s$ is large, the quasihole energies carry essentially no spectral weight. The physical reason for the very small quasihole spectral weight is that interactions are sufficiently strong $1/k_Fa_s \sim O(1)$ and colored fermions are sufficiently nondegenerate ($\mu/E_F \ll -1$) that two-body bound states (colored pairs) are well established. Therefore, the creation of elementary (single-fermion) excitations requires the breaking of two-body bound states and thus only positive-energy states are accessible.

It is important to mention that the color density of states can also be measured using the photoemission spectroscopy technique developed for cold atoms, which was used to probe the density of states of strongly interacting Fermi gas of ^{40}K atoms with two internal states throughout the evolution from the BCS to the BEC limits [61]. Now that we have finalized our discussion of spectroscopic quantities, we would like make some final remarks, before we summarize our conclusions.

VI. FINAL REMARKS

We would like to make some final remarks on a few important issues that we have not discussed so far, such as Efimov states, nonuniform superfluidity, the critical temperature of color superfluids, and trap effects. It is important to understand how these topics are affected by color-orbit and color-flip fields. However, this analysis lies beyond the regions of applicability of our current work, but can be included in refined generalizations as discussed below.

We begin our discussion by pointing out that Efimov trimers in ultracold fermions with three internal states $\{c = R,G,B\}$ can be formed in an extremely dilute cloud of atoms. The densities for which these RGB triatomic molecules may form and remain stable is typically less than 10^{12} atoms

per cubic centimeter, based on an extensive description of Efimov states in a variety of systems [62]. Below the upper bound density for 10^{12} cm^{-3} it may be sufficient to regard the trimers as isolated; however, with increasing atom densities in the range of 10^{12}–10^{14} cm^{-3} the surrounding medium largely limits the formation of stable triatomic molecules. In the particular case of fermions, the Pauli exclusion principle plays an important role as the density increases, eventually preventing the formation of Efimov trimers. If we were to consider that the binding energy of an Efimov RGB trimer was slightly lower than that of dimers RG, GB, and RB and assumed that the lifetime of trimers and dimers were infinitely long, then at low temperatures, a trimer liquid would be expected at lower densities and a dimer superfluid would be expected at higher densities [17,63] in the limit of zero color orbit ($k_T = 0$), color flip ($\Omega = 0$), and color shifts ($\delta = 0$). This situation is similar to what happens in QCD, where at lower densities baryons (RGB trimers of quarks) exist, but at higher densities color superfluids (RG, GB, and RB dimers of quarks) emerge [13,64].

A conjectured zero-temperature phase diagram describing Efimov trimers and color dimers with infinite lifetimes has been sketched for a three-component (color) Fermi mixture in the regime of narrow Feshbach resonances [63], but without color-orbit, color-flip, or color-shift fields. The phase-space parameters used were the resonance strength parameter $k_F R^*$ and the interaction parameter $1/k_F a_s$, where k_F is the Fermi momentum for the three-component system, R^* is the scattering strength length, and a_s is the s-wave scattering length. Indeed, at lower densities Efimov trimers are present, but they dissociate and disappear as density is increased [62,63]. In the broad resonance regime that we are considering, the three-body parameter $\kappa_*^{(0)}$ plays the same role as the inverse of the length associated with the strength of the resonance [62], that is, $(R^*)^{-1}$. Therefore, a similar qualitative phase diagram of $k_F/\kappa_*^{(0)}$ versus $1/k_F a_s$ is expected in the absence of color-orbit and color-flip fields [62,65]. However, the inclusion of color-flip fields creates internal population imbalances, which exacerbate the effects of the Pauli exclusion principle, thus making the formation of Efimov states more difficult. A quantitative analysis of Efimov states for colored fermions with three internal states in the presence of color-orbit and color-flip fields is the subject of another work [65] meant to describe the low-density regime $n \lesssim 10^{12}$ cm^{-3} of the present problem.

However, in the context of cold atoms, the formation of dimers and trimers occurs mostly in excited states and not in their ground states. This means that such excited state dimers and trimers have lifetimes and can decay into lower-energy states spontaneously or dissociate via collisional processes. For instance, the existence of Efimov trimers in ^{6}Li has been observed experimentally via an increase in the particle loss rate mediated by triatomic molecules [9,10] and via atom-dimer loss rates [66,67]. Although, for three-component fermions, we are not aware of experiments that measure directly the lifetimes of excited state dimers and trimers at different scattering lengths, a recent experiment involving ^{85}Rb has shown that excited trimers $^{85}Rb_3{}^*$ have a much shorter lifetime than dimers $^{85}Rb_2{}^*$ with slightly smaller binding energy [68] at various fixed scattering lengths and for densities in the range of 10^{11}–10^{13} atoms/cm^3. For example, in this density interval, lifetimes for trimers range from 125 to 97 μs, while the lifetime of dimers range from 2 to 1 ms at s-wave scattering length $a_s = 700a_0$, where a_0 is the Bohr radius. This indicates that excited dimers can exist about ten times longer than excited trimers with comparable binding energy. If for three-component fermions a similar scenario applies, that is, if at low densities the lifetime of trimers is much shorter than that of dimers with comparable binding energy, then there is a time regime which is sufficiently long for trimers to decay, but sufficiently short for dimers not to decay. In this experimental time regime, we can consider just the quantum phases that emerge due to the existence of atoms and excited dimers, that is, normal state and color-superfluid phases, as discussed in this work. On the other hand, if the lifetimes of dimers and trimers are comparable, it is clear that one must also include possible phases of trimers in the putative phase diagram of three-component fermions.

Another important point to mention is that nonuniform color superfluidity may exist over a narrow area in the BCS regime of the phase diagram shown in Fig. 3, that is, in the range of parameters $\Omega/E_F \lesssim 0.2$ and $1/k_F a_s \lesssim -1$. For continuum problems in three spatial dimensions, nonuniform superfluids occur only in the BCS regime and at very low temperatures $T/T_F \ll 10^{-3}$, as its formation requires a large degree of particle-particle nesting which parabolic bands do not provide [69,70]. Therefore, in three-dimensional continuum systems, nonuniform superfluid states of the Larkin-Ovchinikov [69] or Fulde-Ferrel [70] type may exist only in a very limited region of phase space, which is confined to the BCS regime and very low temperatures. The situation is similar for color superfluids with color-flip and color-orbit fields.

In addition, we would like to comment on the effects of fluctuations and on its importance in obtaining the critical temperature of the system away from the BCS regime. In the case of zero color-orbit and color-flip fields, the critical temperature of color superfluids has been investigated as a function of the interaction parameter $1/k_F a_s$ using the T-matrix approach [16] and leads to results qualitatively similar to those of spin-1/2 Fermi superfluids [59]. Without color-orbit and color-flip fields the normal state of the system evolves from a color (RGB) Fermi liquid to a color Bose liquid with RG, GB, and RB molecules (dimers) of masses M_D equal to twice the mass m of their constituent fermions. The critical temperature in the Bose-Einstein condensation regime is that of noninteracting bosons (dimers) of mass $M_D = 2m$ and density $n_D = n/6$, where n is the density of fermions. Therefore, $T_{\rm BEC} = (2\pi/M_D)[n_D/\zeta(3/2)]^{2/3} = 0.137E_F$ is proportional to Fermi energy.

The critical temperature of spin-1/2 ultracold fermions was recently investigated in the presence of Zeeman fields and of the experimentally relevant equal Rashba-Dresselhaus spin-orbit coupling [71]. That analysis revealed that spin-orbit coupling and Zeeman fields modify the masses of the Bose molecules and lead to an enhancement of the critical temperature in the BEC regime. Furthermore, in the BCS region, the critical temperature lies always below that of a system without Zeeman fields and spin-orbit coupling. A detailed analysis of the fluctuation effects and the critical temperature of color

superfluids in the presence of color-orbit and color-flip fields is an important issue and is left to be carried out later following the works on spin-1/2 fermions [71] and on color superfluids [16].

Finally, we would like to comment on the effects of trapping potentials. Historically, harmonic confining potentials have been consistently used to trap atomic Fermi gases and the local-density approximation (LDA) has been widely used to describe the resulting inhomogeneous states. For harmonic traps $V_{\rm trap}(\mathbf{r})$, the chemical potential μ of our system is mapped onto a local chemical potential $\widetilde{\mu}(\mathbf{r}) = \mu - V_{\rm trap}(\mathbf{r})$ within the LDA. Thus, several of the phases described in our phase diagram, shown in Fig. 3(a), may coexist in a harmonic trap. For example, at unitarity, the single-ring and the three-ring color superfluid phases can coexist in harmonic traps and the detailed inhomogeneous spatial structure of color superfluids needs to be mapped for fixed color-orbit and color-flip fields. However, the current trend in experimental work is to create different types of trapping potentials including that of a box-type variety using digital micromirror devices [72], which can produce homogeneous states. This trend to study experimentally homogeneous systems is reflected in recent work covering both Bose [73] and Fermi [74] atomic superfluids. Thus, we expect that homogeneous color superfluids with and without color-orbit and color-flip fields will be studied using box potentials, such that a direct comparison to our work can be made.

VII. CONCLUSION

We studied the quantum phases of interacting colored fermions in the presence of color-orbit coupling and color-flip fields. Experimental candidates for the observation of such phases include ^{6}Li, ^{40}K, and ^{173}Yb, which possess at least three internal states, which can be labeled red (R), green (G), and blue (B), and therefore can be used to simulate exotic phases related to quantum chromodynamic systems in tabletop experiments.

Among many possibilities of analogous exotic quantum chromodynamic phases, we focused on the emergence of color superfluidity, where the presence of color-orbit coupling and color-flip fields induce Lifshitz-type topological phase transitions. In such transitions, the symmetry of the order parameter tensor does not change, but the structures of the ground-state wave functions and of the energy spectrum of elementary excitations (quasiparticles and quasiholes) do.

We constructed the low-temperature phase diagram of color-flip field versus scattering parameter (interactions) and classified the emerging color superfluid phases in terms of the loci of zeros of the quasiparticle excitation spectrum in momentum space. For fixed color-orbit coupling and quadratic color-shift field, we identified five gapless phases with one, two, three, four, or five rings of nodes in the excitation spectrum and one fully gapped phase. In addition, we found that a very rare quintuple point exists where five gapless superfluid phases with line nodes converge. Given that the phase transitions from one nodal superfluid to another is continuous (second order), the quintuple point is also pentacritical. Furthermore, in the limit of zero color-flip fields but finite color-orbit coupling, phase transitions from the normal state to a nodal superfluid and from a nodal to fully gapped superfluids occur.

We contrasted the phase diagram of nonzero color-orbit coupling with the simpler case of zero color-orbit coupling, where the color-flip field versus scattering parameter phase diagram has only one gapless and one fully gapped superfluid phase. In the limit of zero color-flip field, the gapless phase is described by an inert degenerate mixed-color fermion band and two fully gapped bands of quasiparticle excitations, while the fully gapped phase is described by an inert nondegenerate mixed-color fermion band and two fully gapped bands of quasiparticle excitations. In this case, only a crossover between BCS and BEC superfluids occurs.

We used the connectivity of the nodal regions in momentum space to classify the topology of the superfluid phases and analyzed the order parameter tensor structure in a mixed-color representation as well as in a pseudospin representation exploring the singlet, triplet, and quintet sectors. We found that the nodal structure of the order parameter tensor does not coincide with the nodes in the quasiparticle-quasihole excitation spectrum, which is the case for the more familiar example of spin-1/2 fermions.

In addition to topological aspects, we investigated in detail spectroscopic properties of colored fermions in their normal and superfluid phases. We analyzed the quasiparticle-quasihole excitation spectrum as well as the momentum distribution and density of states of colored fermions and concluded that these properties can be used to help distinguish between different topological nodal phases of color superfluids and can be measured using current experimental techniques.

ACKNOWLEDGMENTS

One of us (C.A.R.S.d.M.) acknowledges the support of the Joint Quantum Institute at the University of Maryland and the National Institute of Standards and Technology, where part of this work was completed during a sabbatical visit, the Galileo Galilei Institute for Theoretical Physics via a Simons Fellowship, and the Aspen Center for Physics via NSF Grant No. PHY1607611.

[1] I. Bloch, Ultracold quantum gases in optical lattices, Nat. Phys. **1**, 23 (2005).

[2] M. Greiner, C. A. Regal, and D. S. Jin, Emergence of a molecular Bose-Einstein condensate from a Fermi gas, Nature (London) **426**, 537 (2003).

[3] K. E. Strecker, G. B. Partridge, and R. G. Hulet, Conversion of an Atomic Fermi Gas to a Long-Lived Molecular Bose Gas, Phys. Rev. Lett. **91**, 080406 (2003).

[4] M. W. Zwierlein, C. A. Stan, C. H. Schunck, S. M. F. Raupach, S. Gupta, Z. Hadzibabic, and W. Ketterle, Observation of

Bose-Einstein Condensation of Molecules, Phys. Rev. Lett. **91**, 250401 (2003).
[5] C. A. Regal, M. Greiner, and D. S. Jin, Observation of Resonance Condensation of Fermionic Atom Pairs, Phys. Rev. Lett. **92**, 040403 (2004).
[6] T. Bourdel, L. Khaykovich, J. Cubizolles, J. Zhang, F. Chevy, M. Teichmann, L. Tarruell, S. J. J. M. F. Kokkelmans, and C. Salomon, Experimental Study of the BEC-BCS Crossover Region in Lithium 6, Phys. Rev. Lett. **93**, 050401 (2004).
[7] M. Bartenstein, A. Altmeyer, S. Riedl, S. Jochim, C. Chin, J. H. Denschlag, and R. Grimm, Crossover from a Molecular Bose-Einstein Condensate to a Degenerate Fermi Gas, Phys. Rev. Lett. **92**, 120401 (2004).
[8] J. Kinast, S. L. Hemmer, M. E. Gehm, A. Turlapov, and J. E. Thomas, Evidence for Superfluidity in a Resonantly Interacting Fermi Gas, Phys. Rev. Lett. **92**, 150402 (2004).
[9] T. B. Ottenstein, T. Lompe, M. Kohnen, A. N. Wenz, and S. Jochim, Collisional Stability of a Three-Component Degenerate Fermi Gas, Phys. Rev. Lett. **101**, 203202 (2008).
[10] J. H. Huckans, J. R. Williams, E. L. Hazlett, R. W. Stites, and K. M. O'Hara, Three-Body Recombination in a Three-State Fermi Gas with Widely Tunable Interactions, Phys. Rev. Lett. **102**, 165302 (2009).
[11] S. Taie, Y. Takasu, S. Sugawa, R. Yamazaki, T. Tsujimoto, R. Murakami, and Y. Takahashi, Realization of a SU(2) × SU(6) System of Fermions in a Cold Atomic Gas, Phys. Rev. Lett. **105**, 190401 (2010).
[12] L. Fallani (private communication).
[13] C. A. R. Sá de Melo, When fermions become bosons: Pairing in ultracold gases, Phys. Today **61**(10), 45 (2008).
[14] L. He, M. Jin, and P. Zhuang, Superfluidity in a three-flavor Fermi gas with SU(3) symmetry, Phys. Rev. A **74**, 033604 (2006).
[15] R. W. Cherng, G. Refael, and E. Demler, Superfluidity and Magnetism in Multicomponent Ultracold Fermions, Phys. Rev. Lett. **99**, 130406 (2007).
[16] T. Ozawa and G. Baym, Population imbalance and pairing in the BCS-BEC crossover of three-component ultracold fermions, Phys. Rev. A **82**, 063615 (2010).
[17] A. Rapp, G. Zarand, C. Honerkamp, and W. Hofstetter, Color Superfluidity and "Baryon" Formation in Ultracold Fermions, Phys. Rev. Lett. **98**, 160405 (2007).
[18] B. Barrois, Superconducting quark matter, Nucl. Phys. B **129**, 390 (1977).
[19] D. Bailin and A. Love, Superfluidity and superconductivity in relativistic fermion systems, Phys. Rep. **107**, 325 (1984).
[20] R. Rapp, T. Schäfer, E. V. Shuryak, and M. Velkovsky, Diquark Bose Condensates in High Density Matter and Instantons, Phys. Rev. Lett. **81**, 53 (1998).
[21] M. Alford, K. Rajagopal, and F. Wilczek, QCD at finite baryon density: Nucleon droplets and color superconductivity, Phys. Lett. B **422**, 247 (1998).
[22] I. A. Shovkovy and L. C. Wijewardhana, On gap equations and color-flavor locking in cold dense QCD with three massless flavors, Phys. Lett. B **470**, 189 (1999).
[23] R. Rapp, T. Schäfer, E. V. Shuryak, and M. Velkovsky, High-density QCD and instantons, Ann. Phys. (NY) **280**, 35 (2000).
[24] T. Schäfer, Patterns of symmetry breaking in QCD at high baryon density, Nucl. Phys. B **575**, 269 (2000).
[25] N. Evans, J. Hormuzdiar, S. D. Hsu, and M. Schwetz, On the QCD ground state at high density, Nucl. Phys. B **581**, 391 (2000).
[26] J. Hosek, Macroscopic quantum phases of a deconfined QCD matter at finite density, arXiv:hep-ph/9812516.
[27] T. Schäfer, Quark hadron continuity in QCD with one flavor, Phys. Rev. D **62**, 094007 (2000).
[28] J. Hosek, Anisotropic color superconductor, arXiv:hep-ph/0011034.
[29] C. Schaab, B. Hermann, F. Weber, and M. K. Weigel, Differences in the cooling behavior of strange quark matter stars and neutron stars, Astrophys. J. Lett. **480**, L111 (1997).
[30] D. Blaschke, T. Klahn, and D. N. Voskresensky, Diquark condensates and compact star cooling, Astrophys. J. **533**, 406 (2000).
[31] D. Page, M. Prakash, J. M. Lattimer, and A. W. Steiner, Prospects of Detecting Baryon and Quark Superfluidity from Cooling Neutron Stars, Phys. Rev. Lett. **85**, 2048 (2000).
[32] M. Alford, J. Bowers, and K. Rajagopal, Crystalline color superconductivity, Phys. Rev. D **63**, 074016 (2001).
[33] L. F. Livi, G. Cappellini, M. Diem, L. Franchi, C. Clivati, M. Frittelli, F. Levi, D. Calonico, J. Catani, M. Inguscio, and L. Fallani, Synthetic Dimensions and Spin-Orbit Coupling with an Optical Clock Transition, Phys. Rev. Lett. **117**, 220401 (2016).
[34] Y. J. Lin, K. Jimenez-Garcia, and I. B. Spielman, Spin-orbit-coupled Bose-Einstein condensates, Nature (London) **471**, 83 (2011).
[35] C. J. Wu, I. M. Shem, and X. F. Zhou, Unconventional Bose-Einstein condensations from spin-orbit coupling, Chin. Phys. Lett. **28**, 097102 (2011).
[36] T. L. Ho and S. Zhang, Bose-Einstein Condensates with Spin-Orbit Interaction, Phys. Rev. Lett. **107**, 150403 (2011).
[37] Y. Li, L. P. Pitaevskii, and S. Stringari, Quantum Tricriticality and Phase Transitions in Spin-Orbit Coupled Bose-Einstein Condensates, Phys. Rev. Lett. **108**, 225301 (2012).
[38] R. A. Williams, M. C. Beeler, L. J. LeBlanc, K. Jimenez-Garcia, and I. B. Spielman, Raman-Induced Interactions in a Single-Component Fermi Gas Near an *s*-Wave Feshbach Resonance, Phys. Rev. Lett. **111**, 095301 (2013).
[39] Z. Fu, L. Huang, Z. Meng, P. Wang, L. Zhang, S. Zhang, H. Zhai, P. Zhang, and J. Zhang, Production of Feshbach molecules induced by spin-orbit coupling in Fermi gases, Nat. Phys. **10**, 110 (2014).
[40] M. Chapman and C. Sá de Melo, Atomic physics: Atoms playing dress-up, Nature (London) **471**, 41 (2011).
[41] J. P. Vyasanakere, S. Zhang, and V. B. Shenoy, BCS-BEC crossover induced by a synthetic non-Abelian gauge field, Phys. Rev. B **84**, 014512 (2011).
[42] M. Gong, S. Tewari, and C. Zhang, BCS-BEC Crossover and Topological Phase Transition in 3D Spin-Orbit Coupled Degenerate Fermi Gases, Phys. Rev. Lett. **107**, 195303 (2011).
[43] Z.-Q. Yu and H. Zhai, Spin-Orbit Coupled Fermi Gases across a Feshbach Resonance, Phys. Rev. Lett. **107**, 195305 (2011).
[44] H. Hu, L. Jiang, X.-J. Liu, and H. Pu, Probing Anisotropic Superfluidity in Atomic Fermi Gases with Rashba Spin-Orbit Coupling, Phys. Rev. Lett. **107**, 195304 (2011).
[45] L. Han and C. A. R. Sá de Melo, Evolution from BCS to BEC superfluidity in the presence of spin-orbit coupling, Phys. Rev. A **85**, 011606(R) (2012).
[46] K. Seo, L. Han, and C. A. R. Sá de Melo, Emergence of Majorana and Dirac Particles in Ultracold Fermions via Tunable Interactions, Spin-Orbit Effects, and Zeeman Fields, Phys. Rev. Lett. **109**, 105303 (2012).

[47] J. P. A. Devreese, J. Tempere, and C. A. R. Sá de Melo, Effects of Spin-Orbit Coupling on the Berezinskii-Kosterlitz-Thouless Transition and the Vortex-Antivortex Structure in Two-Dimensional Fermi Gases, Phys. Rev. Lett. **113**, 165304 (2014).
[48] I. B. Spielman (private communication).
[49] N. Goldman, I. Satija, P. Nikolic, A. Bermudez, M. A. Martin-Delgado, M. Lewenstein, and I. B. Spielman, Realistic Time-Reversal Invariant Topological Insulators with Neutral Atoms, Phys. Rev. Lett. **105**, 255302 (2010).
[50] I. M. Lifshitz, Anomalies of electron characteristics of a metal in the high pressure region, Zh. Eksp. Teor. Fiz. **38**, 1569 (1960) [Sov. Phys. JETP **11**, 1130 (1960)].
[51] R. P. Feynman, *Feynman Lectures in Physics* (Pearson/Addison-Wesley, Reading, 1963), Vol. 3, Chap. 15.
[52] D. L. Campbell, R. M. Price, A. Putra, A. Valdés-Curiel, D. Trypogeorgos, and I. B. Spielman, Magnetic phases of spin-1 spin-orbit-coupled Bose gases, Nat. Commun. **7**, 10897 (2016).
[53] J. R. Engelbrecht, M. Randeria, and C. A. R. Sá de Melo, BCS to Bose crossover: Broken-symmetry state, Phys. Rev. B **55**, 15153 (1997).
[54] G. Cardano, *The Rules of Algebra (Ars Magna)* (Dover, New York, 2007).
[55] K. Enomoto, K. Kasa, M. Kitagawa, and Y. Takahashi, Optical Feshbach Resonance Using the Intercombination Transition, Phys. Rev. Lett. **101**, 203201 (2008).
[56] R. Yamazaki, S. Taie, S. Sugawa, and Y. Takahashi, Submicron Spatial Modulation of an Interatomic Interaction in a Bose-Einstein Condensate, Phys. Rev. Lett. **105**, 050405 (2010).
[57] D. M. Kurkcuoglu and C. A. R. Sá de Melo, Quantum phases of interacting three-component fermions under the influence of spin-orbit coupling and Zeeman fields, arXiv:1612.02365v1.
[58] D. M. Kurkcuoglu and C. A. R. Sá de Melo, Creating spin-one fermions in the presence of artificial spin-orbit fields: Emergent spinor physics and spectroscopic properties, J. Low Temp. Phys. (2018), doi:10.1007/s10909-018-1852-0
[59] C. A. R. Sá de Melo, M. Randeria, and J. R. Engelbrecht, Crossover from BCS to Bose Superconductivity: Transition Temperature and Time Dependent Ginzburg-Landau Theory, Phys. Rev. Lett. **71**, 3202 (1993).
[60] A. M. Clogston, Upper Limit for the Critical Field in Hard Superconductors, Phys. Rev. Lett. **9**, 266 (1962).
[61] J. T. Stewart, J. P. Gaebler, and D. S. Jin, Using photoemission spectroscopy to probe a strongly interacting Fermi gas, Nature (London) **454**, 744 (2008).
[62] P. Naidon and S. Endo, Efimov physics: A review, Rep. Prog. Phys. **80**, 056001 (2017).
[63] Y. Nishida, New Type of Crossover Physics in Three-Component Fermi Gases, Phys. Rev. Lett. **109**, 240401 (2012).
[64] M. G. Alford, A. Schmitt, K. Rajagopal, and T. Schäfer, Color superconductivity in dense quark matter, Rev. Mod. Phys. **80**, 1455 (2008).
[65] D. M. Kurkcuoglu and C. A. R. Sá de Melo (unpublished).
[66] T. Lompe, T. B. Ottenstein, F. Serwane, K. Viering, A. N. Wenz, G. Zürn, and S. Jochim, Atom-Dimer Scattering in a Three-Component Fermi Gas, Phys. Rev. Lett. **105**, 103201 (2010).
[67] S. Nakajima, M. Horikoshi, T. Mukaiyama, P. Naidon, and M. Ueda, Nonuniversal Efimov Atom-Dimer Resonances in a Three-Component Mixture of ^{6}Li, Phys. Rev. Lett. **105**, 023201 (2010).
[68] C. E. Klauss, X. Xie, C. Lopez-Abadia, J. P. D'Incao, Z. Hadzibabic, D. S. Jin, and E. A. Cornell, Observation of Efimov Molecules Created from a Resonantly Interacting Bose Gas, Phys. Rev. Lett. **119**, 143401 (2017).
[69] A. I. Larkin and Y. N. Ovchinnikov, Inhomogeneous states of superconductors, Zh. Eksp. Teor. Fiz. **47**, 1136 (1964) [Sov. Phys. JETP **20**, 762 (1965)].
[70] P. Fulde and R. A. Ferrel, Superconductivity in a strong spin-exchange field, Phys. Rev. **135**, A550 (1964).
[71] P. D. Powell, G. Baym, and C. A. R. Sá de Melo, Superfluid transition temperature of spin-orbit and Rabi coupled fermions with tunable interactions, arXiv:1709.07042v1.
[72] G. Gauthier, I. Lenton, N. McKay Parry, M. Baker, M. J. Davis, H. Rubinsztein-Dunlop, and T. W. Neely, Direct imaging of a digital-micromirror device for configurable microscopic optical potentials, Optica **3**, 1136 (2016).
[73] R. Lopes, C. Eigen, N. Navon, D. Clement, R. P. Smith, and Z. Hadzibabic, Quantum Depletion of a Homogeneous Bose-Einstein Condensate, Phys. Rev. Lett. **119**, 190404 (2017).
[74] B. Mukherjee, Z. Yan, P. B. Patel, Z. Hadzibabic, T. Yefsah, J. Struck, and M. W. Zwierlein, Homogeneous Atomic Fermi Gases, Phys. Rev. Lett. **118**, 123401 (2017).